2016-06

FREE SPACE LASER COMMUNICATIONS AND APPLICATIONS

Onuk, Selcuk

Monterey, California. Naval Postgraduate School

NAVAL POSTGRADUATE SCHOOL

MONTEREY, CALIFORNIA

THESIS

FREE SPACE LASER COMMUNICATIONS AND APPLICATIONS

by

Selcuk Onuk

June 2016

Thesis Advisor: Tri T. Ha
Co-Advisor: Weilian Su

Approved for public release; distribution is unlimited

THIS PAGE INTENTIONALLY LEFT BLANK

REPORT DOCUMENTATION PAGE			*Form Approved OMB No. 0704-0188*

1. AGENCY USE ONLY *(Leave blank)*	**2. REPORT DATE** June 2016	**3. REPORT TYPE AND DATES COVERED** Master's Thesis

4. TITLE AND SUBTITLE
FREE SPACE LASER COMMUNICATIONS AND APPLICATIONS

5. FUNDING NUMBERS

6. AUTHOR(S) Selcuk Onuk

7. PERFORMING ORGANIZATION NAME(S) AND ADDRESS(ES)
Naval Postgraduate School
Monterey, CA 93943-5000

8. PERFORMING ORGANIZATION REPORT NUMBER

9. SPONSORING /MONITORING AGENCY NAME(S) AND ADDRESS(ES)
N/A

10. SPONSORING / MONITORING AGENCY REPORT NUMBER

11. SUPPLEMENTARY NOTES The views expressed in this thesis are those of the author and do not reflect the official policy or position of the Department of Defense or the U.S. Government. IRB Protocol number ____N/A____.

12a. DISTRIBUTION / AVAILABILITY STATEMENT	**12b. DISTRIBUTION CODE**
Approved for public release; distribution is unlimited	A

13. ABSTRACT (maximum 200 words)

Optical communications offer many advantages over radio frequency communications. Lasers are very efficient in establishing a communication link; however, they have a major drawback, which is background radiation, because background radiation limits the efficiency of optical communications.

In this thesis, we analyze inexpensive lasers and their vulnerabilities to background radiation. We present a new way of calculating background radiation by using measured data and Planck's Law. Next, we consider how to maximize the bit rate of a communication link for inexpensive lasers. We also investigate several modulation types for optical communication. We present M-ary pulse-position modulation (MPPM) and a novel method of direct detection. Next, we compare MPPM with on-off keying (OOK) in terms of power requirements. It is shown that MPPM is much more power efficient than OOK modulation; 32-PPM requires 7.6 dB less power than OOK to achieve the same probability of bit error. We use Simulink to model MPPM performance, and we compare analytical results with simulated results.

14. SUBJECT TERMS optical communication, background radiation, pulse-position modulation, on-off keying, intensity modulation, direct detection	**15. NUMBER OF PAGES** 81
	16. PRICE CODE

17. SECURITY CLASSIFICATION OF REPORT	**18. SECURITY CLASSIFICATION OF THIS PAGE**	**19. SECURITY CLASSIFICATION OF ABSTRACT**	**20. LIMITATION OF ABSTRACT**
Unclassified	Unclassified	Unclassified	UU

NSN 7540-01-280-5500

Standard Form 298 (Rev. 2-89)
Prescribed by ANSI Std. 239-18

THIS PAGE INTENTIONALLY LEFT BLANK

Approved for public release; distribution is unlimited

FREE SPACE LASER COMMUNICATIONS AND APPLICATIONS

Selcuk Onuk
Lieutenant Junior Grade, Turkish Navy
B.S., Turkish Naval Academy, 2010

Submitted in partial fulfillment of the
requirements for the degree of

MASTER OF SCIENCE IN ELECTRICAL ENGINEERING

from the

NAVAL POSTGRADUATE SCHOOL
June 2016

Approved by: Tri T. Ha
Thesis Advisor

Weilian Su
Co-Advisor

Clark R. Robertson
Chair, Department of Electrical and Computer Engineering

THIS PAGE INTENTIONALLY LEFT BLANK

ABSTRACT

Optical communications offer many advantages over radio frequency communications. Lasers are very efficient in establishing a communication link; however, they have a major drawback, which is background radiation, because background radiation limits the efficiency of optical communications.

In this thesis, we analyze inexpensive lasers and their vulnerabilities to background radiation. We present a new way of calculating background radiation by using measured data and Planck's Law. Next, we consider how to maximize the bit rate of a communication link for inexpensive lasers. We also investigate several modulation types for optical communication. We present *M*-ary pulse-position modulation (*M*PPM) and a novel method of direct detection. Next, we compare *M*PPM with on-off keying (OOK) in terms of power requirements. It is shown that *M*PPM is much more power efficient than OOK modulation; 32-PPM requires 7.6 dB less power than OOK to achieve the same probability of bit error. We use Simulink to model *M*PPM performance, and we compare analytical results with simulated results.

THIS PAGE INTENTIONALLY LEFT BLANK

TABLE OF CONTENTS

LIST OF FIGURES

LIST OF TABLES

THIS PAGE INTENTIONALLY LEFT BLANK

LIST OF ACRONYMS AND ABBREVIATIONS

APD	Avalanche-Photo Diode
AWGN	Additive White Gaussian Noise
BER	Bit Error Ratio
DPPM	Differential Pulse-Position Modulation
FCC	Federal Communications Commission
FOV	Field-of-View
FSO	Free Space Optical
IM/DD	Intensity Modulation/Direct Detection
*M*PPM	*M*-ary Pulse-Position Modulation
OFDM	Orthogonal-Frequency Division Multiplexing
OOK	On-Off Keying
OPALS	Optical Payload for Lasercomm Science
PAM	Pulse-Amplitude Modulation
PIN	Photo-Intrinsic Negative
PPM	Pulse-Position Modulation
PSK	Phase-Shift Keying
PWM	Pulse-Width Modulation
QPSK	Quadrature Phase-Shift Keying
RF	Radio Frequency
SNR	Signal-to-Noise Ratio
UAV	Unmanned Air Vehicle

THIS PAGE INTENTIONALLY LEFT BLANK

ACKNOWLEDGMENTS

I would like to thank my advisor, Professor Tri Ha, for his explanations, help, guidance, and patience. He always gave me self-confidence and courage in writing this thesis.

I want to thank Bob Broadston and my co-advisor, Professor Weilian Su, for their help with the simulation.

I want to thank my big brother for his recommendations about life in the United States. I am also thankful to my family for their continuous support.

Finally, I am grateful to the Turkish Navy, my superiors, and friends for giving me the opportunity and helping me to be a graduate student at the Naval Postgraduate School.

THIS PAGE INTENTIONALLY LEFT BLANK

I. INTRODUCTION

A. BACKGROUND

Free space optical communications offers many advantages over radio frequency communications. These advantages include interference-free communications, a high bit rate communications link, low power requirements, smaller antenna sizes, and fewer bandwidth constraints. The bandwidth for optical communications is unregulated, and bandwidth approval from the Federal Communications Commission (FCC) is not required [1]; however, free space optical communication is adversely affected by background radiation, which is mostly caused by sunlight. This radiation limits the range of optical communications. Furthermore, optical communication links using lasers can only be used for line-of-sight applications. Unlike radio frequency (RF) signals, optical signal cannot go through walls. Additionally, optical communications in atmospheric channels are affected by atmospheric and weather conditions such as fog, rain, snow, absorption and scattering.

Background radiation includes solar radiation and earth radiation, which is caused by the reflection of solar radiation from the Earth's surface as well as radiations reflected from planets and stars. Solar radiation is the biggest radiation problem for lasers as compared with other radiation sources. Background radiation is modeled using Planck's Law for black-body radiation and does not take atmospheric conditions into consideration.

On-Off keying (OOK) and pulse-position modulation (PPM) are the most commonly used modulation techniques for optical communications. OOK offers simple modulation with on and off pulses; however, OOK requires more signal power than PPM. *M*-ary pulse-position modulation (*M*PPM) is a variation of PPM. When it is employed with large *M*, its power efficiency makes it preferable to OOK.

There are two types of detection methods for optical communication. Coherent detection uses a local oscillator during the demodulation process. The phases, polarization, and amplitudes of the received signal are detected with coherent detection.

Direct detection does not use a local oscillator to demodulate the received signal. Instead, the amplitude of the signal is detected. The polarization and phase of the signal are lost at the receiver; therefore, direct detection must be used with intensity modulation. Implementation of direct detection is simpler, cost effective, and eliminates the need for a local oscillator [2].

There are two types of photo diodes used in optical communication, photo-intrinsic negative (PIN) and avalanche-photo diodes (APD). PIN diodes are low cost and widely available but have less internal gain than APD diodes. APD diodes are expensive and have temperature control problems [3].

Wavelength choice is a key factor in optical communication. Wavelengths of 600 nm and 1550 nm are the most widely used wavelengths [2]. Eye and skin safety regulations limit the wavelength usage. Optical signals with a 600 nm wavelength can transmit more power than signals with a wavelength of 1550 nm; however, the 600 nm wavelength signal is considered to be harmful to the human eye if it is used at high power. As a result, the 1550 nm wavelength signal is widely used in commercial optical devices [4].

Average power is an important factor to consider in optical communications as well and is used to compare the performance of optical modulation techniques [5].

Optical communication can be used for various applications. These applications include [1]:

- Communications between ground station and Unmanned Air Vehicles (UAV),
- Communications between ground station and satellite,
- Communications between satellites, and
- Secure and interference-free communications between ships with high bit rates.

The interference-free feature of optical communications is a result of its narrow beamwidth. Additionally, a receiver in the optical communication link must be aware of the optical signal’s presence prior to link establishment. In other words, the receiver must

know where and when to look for the incoming signal. This makes it very secure and attractive for military applications.

An optical communications link can be established for very long distances depending on the transmit laser and the receiver used. NASA's successful Optical Payload for Lasercomm Science (OPALS) experiment to establish a communications link between Earth and International Space Station (ISS) in 2014 demonstrates the application of this type of communications link [6]. Optical communications is a good candidate as an alternative to radio frequency communications.

B. THESIS OBJECTIVES

There are three objectives of this thesis. The first is to carry out an optical communications link budget analysis, determine the appropriate signal wavelength, and find the limit of optical communications link distance in the presence of background radiation for low power and inexpensive lasers. The second objective is to find the appropriate modulation scheme for low power and inexpensive lasers and compare them theoretically. The third objective is to simulate the appropriate modulation scheme using Simulink to compare theoretical results with simulated results.

C. THESIS ORGANIZATION

This thesis is organized into five chapters including the introduction, Chapter I. Background radiation, link analysis, and comparisons for different signal wavelengths are presented in Chapter II. We analyze an optical communications link with inexpensive lasers using low power. Additionally, we correlate the calculation of background radiation between Planck's Law and measured values. Furthermore, we examine and try to maximize the optical communications bit rate and distance for different wavelengths. We demonstrate that optical communications with a bit rate of 882 Mb/s is theoretically possible at up to 3 km using inexpensive lasers.

In Chapter III, *M*-ary PPM modulation and demodulation with direct detection are introduced, and *M*-ary PPM and OOK modulation are compared. We find that *M*-ary PPM modulation uses much less power than OOK for the same bit rate and probability of

bit error when *M* is large. We also present a novel method of demodulation for *M*-ary PPM with direct detection using threshold detectors. This method offers simplicity and robustness. We present the necessary equations for *M*-ary PPM with direct detection and their derivations for this new method. Additionally, we compare *M*-ary PPM with OOK modulation in terms of power requirements and probability of bit error. We show that *M*-ary PPM requires less power than OOK modulation for the same probability of bit error.

In Chapter IV, *M*-ary PPM modulation and direct detection are simulated in Simulink in order to confirm the theoretical results with simulation. Simulink models of *M*-ary PPM modulation and direct detection links for different *M* are presented. *M*-ary PPM and OOK are compared in terms of power efficiency using both theoretical and simulation results.

Finally, the conclusion of the thesis and recommendations for future work are discussed in Chapter V.

II. LINK ANALYSIS

A. FREE-SPACE OPTICAL COMMUNICATION

The link analysis estimates the received optical power P_r, given the transmitter power P_t, the distance *d* between the transmitter and the receiver, the optical signal wavelength λ, the transmit optical antenna gain G_t and the receiver optical antenna gain G_r. The power of background radiation, or noise from the Sun, moon, planets, stars, and sky, is also included in link analysis calculation. The received signal-to-noise ratio (SNR) can be calculated after considering those elements.

1. Received Power

The received optical power is calculated from

$$P_r = \frac{P_t G_t G_r \eta_t \eta_r}{L_{fs} L_a L_p}, \tag{2-1}$$

where free space loss L_{fs} is calculated by the Friis' formula

$$L_{fs} = \left(\frac{4\pi d}{\lambda} \right)^2, \tag{2-2}$$

and η_t and η_r are the efficiencies of the transmitter and receiver optics, respectively; the parameter L_a is the atmospheric loss, and L_p is the pointing loss.

2. Transmit Antenna Gain

Transmit antenna gain G_t for a laser beam is calculated from [7]

$$G_t = 8\left(\frac{\pi \omega_0}{\lambda} \right)^2, \tag{2-3}$$

where ω_0 is the radius of the optical beam and is typically a few mm [8]. It can also be expressed in terms of the optical beam divergence angle θ in the far-field for a laser beam as [7]

$$G_t = \frac{32}{\theta^2} \approx 16\left(\frac{D_t}{\lambda}\right)^2, \tag{2-4}$$

where

$$\theta = \frac{2\lambda}{\pi\omega_0} \approx \sqrt{2}\frac{\lambda}{\pi\omega_0/\sqrt{2}} = \sqrt{2}\frac{\lambda}{D_t}, \tag{2-5}$$

the half-angle $\theta/2$ is defined as the angle from the optical axis to the $1/e^2$ intensity points of a Gaussian beam, and D_t is the diameter of the aperture of the transmit circular lens antenna [9].

Consider an optical transmitter that emits a laser beam with a divergence angle $\theta = 0.83$ mrd. The wavelength is $\lambda = 1550$ nm. The diameter of the aperture of the transmit circular lens antenna is $D_t = 2.64$ mm. The on-axis gain of the laser beam G_t is calculated using (2-4) as 76.67 dB.

The transmit optical antenna gain G_t of a Cassegrain antenna is given by [7]

$$G_t = \frac{4\pi A_t}{\lambda^2}\eta_t(\alpha), \tag{2-6}$$

where

$$A_t = \frac{\pi D_t^2}{4} \tag{2-7}$$

is the aperture of the Cassegrain antenna with diameter D_t. The efficiency $\eta_t(\alpha)$ is calculated from

$$\eta_t(\alpha) = \frac{2}{\alpha^2}\left(\mathrm{e}^{-\alpha^2} - e^{-\gamma^2\alpha^2}\right)^2, \tag{2-8}$$

where α is the aperture-to-beamwidth ratio and γ is the obscuration ratio. The aperture radius-to-beamwidth ratio is $\alpha = a/\omega$, where a is the primary mirror radius and beamwidth ω is the distance from the antenna axis to the $1/e^2$ intensity points of the Gaussian optical beam. The obscuration ratio γ is calculated from b/a, where b is the secondary mirror radius (obscuration radius). An approximation for α is given by [9]

$$\alpha = 1.12 - 1.3\gamma^2 + 2.12\gamma^4. \tag{2-9}$$

Consider a Cassegrain optical antenna with a primary mirror radius $a = 10$ cm (centimeters) and secondary mirror radius $b = 2$ cm. The antenna is illuminated by a laser operating in a Gaussian mode at wavelength $\lambda = 1550$ nm. From (2-6), (2-8), and (2-9), we get the obscuration ratio as $\gamma = b/a = 2/10 = 0.2$, the beamwidth ratio $\alpha = 1.0714$ and $\eta_t(\alpha) = 0.928$, so $G_t = 106$ dB.

3. Receive Antenna Gain

The receive optical antenna gain G_r is given by

$$G_r = \eta_r \frac{4\pi A_r}{\lambda^2}, \tag{2-10}$$

where A_r is the aperture of the receive-optical antenna, η_r is the receive antenna efficiency, and λ is the wavelength of an optical signal. The value A_r can be calculated for a circular aperture of diameter D_r from

$$A_r = \frac{\pi D_r^2}{4}. \tag{2-11}$$

Antenna efficiency for a Cassegrain optical antenna with primary mirror diameter $D_r = 2a$ and secondary mirror diameter $d_r = 2b$ is given by [7]

$$\eta_r = 1 - \gamma^2 \tag{2-12}$$

where

$$\gamma = \frac{d_r}{D_r} = \frac{b}{a}. \tag{2-13}$$

The gain G_r of a Cassegrain optical antenna can also be expressed as

$$G_r = (1-\gamma^2)\left(\frac{\pi D_r}{\lambda}\right)^2. \tag{2-14}$$

Consider the gain of the Cassegrain optical antenna when it is used as the receive-optical antenna which $D_r = D_t$; we obtain

$$\frac{G_r}{G_t} = \frac{(1-\gamma^2)\left(\frac{\pi D_r}{\lambda}\right)^2}{16\left(\frac{D_t}{\lambda}\right)^2} = \frac{\pi^2}{16}(1-\gamma^2). \tag{2-15}$$

If the obscuration ratio $\gamma = 0.2$, then the gain G_r is 2.3 dB less than the gain G_t. If the transmit antenna gain is 106 dB as in the previous example, the receive antenna gain is 103.7 dB.

Consider a free-space laser link using Cassegrain optical transmit and receive antennas as described in the previous examples. The transmit power is $P_t = 4$ mW, or -24 dBW, the transmitter and receiver optical efficiencies are $\eta_t = 0.63$, or 2 dB, and $\eta_r = 0.5$, or 3 dB. The atmospheric loss is $L_a = 3$ dB, and the pointing loss is negligible. The received power-distance product is obtained by substituting (2-2) into (2-1). We get $P_r d^2 = 8912.5$ and $P_r = 2.22$ mW for $d = 2$ km.

If the transmitter bypasses the Cassegrain optical antenna altogether and instead uses the natural divergence of the laser beam with the on-axis gain of $G_t = 76.67$ dB, then the received power-distance product is obtained by substituting (2-2) into (2-1). We get $P_r d^2 = 10.4$ and $P_r = 2.6\,\mu$W for $d = 2$ km.

4. Background Radiation

The optical signal that arrives at the receiver is accompanied by unwanted light from celestial bodies in a free-space optical (FSO) space-ground communication link. A black body in thermal equilibrium at temperature T_B emits electromagnetic radiation at all wavelengths. The units of the spectral radiance, or spectral brightness $I_\lambda(T_B)$ of black body, are $W \cdot sr^{-1} \cdot m^{-3}$. The spectral radiance is given by Planck's Law as [10]

$$I_\lambda(T_B) = \frac{2hc^2}{\lambda^5}\frac{1}{e^{hc/\lambda kT_B} - 1}, \tag{2-16}$$

where the Wien approximation for shorter wavelengths is

$$I_\lambda(T_B) = \frac{2hc^2}{\lambda^5} e^{-hc/\lambda kT_B},\ hc \gg \lambda kT_B, \tag{2-17}$$

and Boltzmann's constant k is 1.38×10^{-23} J/K, Planck's constant h is $6.626\times10^{-34}\ J\cdot s$, the speed of light c is 3×10^{8} m/s, and T_B is the black body's absolute temperature measured in Kelvin.

The FSO space-ground communications link spectral radiance changes as the wavelength changes. We see in Figure 1 that as wavelength shortens, the spectral radiance increases.

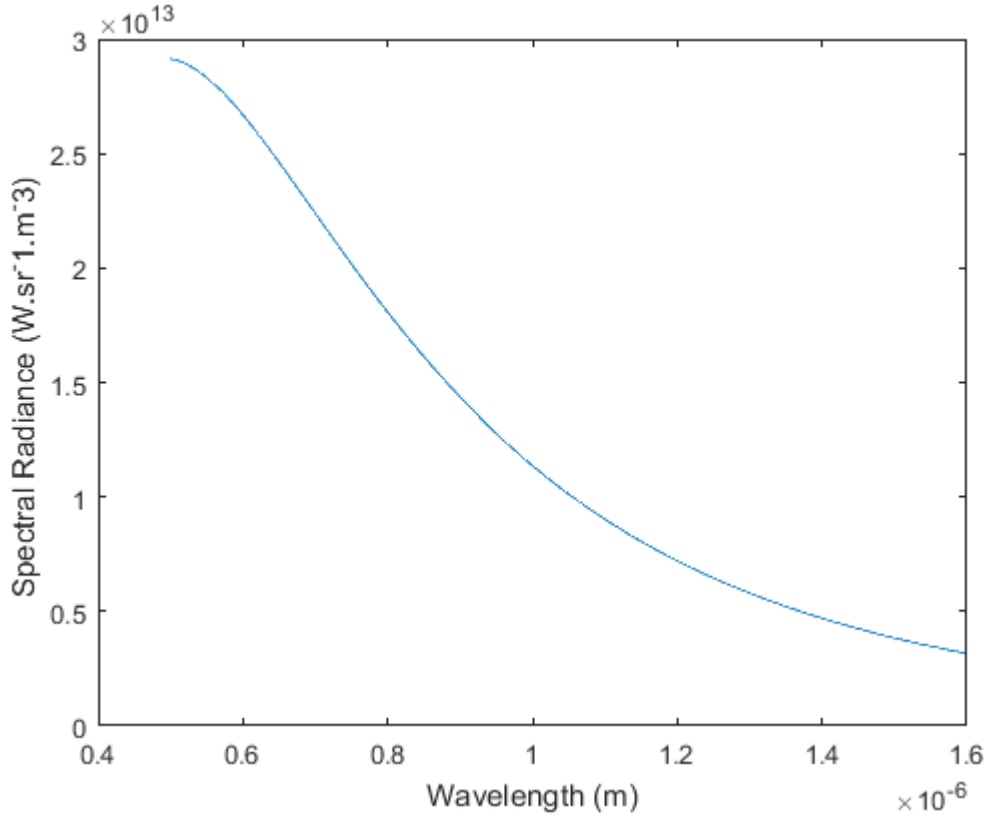

Figure 1. Spectral Radiance of the Sun

The power spectral density of the spectral radiance of the black body in W/m at the receive-optical antenna of diameter D_r is given by [10]

$$N_{0,\lambda}(T_B) = \frac{A_B}{d_B^2}\frac{\pi D_r^2}{4} I_\lambda(T_B), \tag{2-18}$$

where units of $N_{0,\lambda}(T_B)$ are W/m, the distance d_B between the receive-optical antenna and the black body is in meters, A_B is the area of the black body seen by the optical antenna, and the ratio A_B / d_B^2 in steradians is the solid angle subtends by the black body.

Consider an FSO communication link operating at $\lambda = 1550$ nm with a receive-optical antenna of diameter D_r. The spectral radiance at the receive-optical antenna from background radiation of a black body at temperature $T_B = 300$ K is calculated from (2-16) as $I_\lambda(T_B) = 0.4695\ W \cdot sr^{-1} \cdot m^{-3}$.

If the θ_{FOV} is the planar angular of the receiver field-of-view (FOV), the area A_B of the black body seen by the optical antenna is given by [2]

$$A_B = \frac{\pi \theta_{FOV}^2 d_B^2}{4} \tag{2-19}$$

when

$$\Omega_B = \frac{\pi D_B^2}{4 d_B^2} > \Omega_{FOV} = \frac{\pi \theta_{FOV}^2}{4}, \tag{2-20}$$

which is equivalent to

$$\frac{D_B}{d_B} > \theta_{FOV}, \tag{2-21}$$

or

$$A_B = \frac{\pi D_B^2}{4} \tag{2-22}$$

when

$$\Omega_B < \Omega_{FOV}, \tag{2-23}$$

where Ω_B is the solid angle subtended by source, D_B is the diameter of source, and Ω_{FOV} is the receiver field-of-view. The power spectral density at the receive-optical antenna of diameter D_r is given by [2]

$$N_{0,\lambda}(T_B) = \frac{\pi\theta_{FOV}^2}{4}\frac{\pi D_r^2}{4} I_\lambda(T_B) \tag{2-24}$$

when

$$\Omega_B = \frac{\pi D_B^2}{4d_B^2} > \Omega_{FOV} = \frac{\pi\theta_{FOV}^2}{4}, \tag{2-25}$$

and

$$N_{0,\lambda}(T_B) = \frac{\pi D_B^2}{4d_B^2}\frac{\pi D_r^2}{4} I_\lambda(T_B) \tag{2-26}$$

when

$$\Omega_B < \Omega_{FOV}. \tag{2-27}$$

However, in the optical regime we have to take into account the existence of mutually independent spatial modes. The received data field is assumed to be single mode, as it originates from a distant point source. The number of background modes the receiver sees, *m*, will be greater than unity if the receiver's actual field-of-view Ω_{FOV} is larger than its diffraction limited value Ω_{DL}. [11]

The number of spatial mode m is given by [11]

$$m = \begin{cases} \dfrac{\Omega_{FOV}}{\Omega_{DL}} & \Omega_B > \Omega_{FOV} \\ \dfrac{\Omega_B}{\Omega_{DL}} & \Omega_B < \Omega_{FOV} \end{cases}. \tag{2-28}$$

The solid angle subtended by source Ω_B is larger than the receiver field-of-view Ω_{FOV} in (2-24). We use $m = \Omega_{FOV} / \Omega_{DL}$ in (2-28) and $\Omega_{DL} = 4\lambda^2 / D_r^2\pi$ with $\theta_{FOV} = \theta_{DL}$ since this applies to all bodies consistent with reasonable receiver diameters for the diffraction-limited case [12], which implies $m = 1$. The power spectral density per wavelength for the diffraction-limited case is [2]

$$N_{0,\lambda}(T_B) = \lambda^2 m I_\lambda(T_B). \tag{2-29}$$

When $m = 1$, we get

$$N_{0,\lambda}(T_B) = \lambda^2 I_\lambda(T_B) \tag{2-30}$$

when

$$\Omega_B > \Omega_{FOV}. \tag{2-31}$$

Substituting (2-16) into (2-30), we get

$$N_{0,\lambda}(T_B) = \frac{2hc^2}{\lambda^3}\frac{1}{e^{hc/\lambda kT_B} - 1}. \tag{2-32}$$

Consider the Earth to be the black body and an optical antenna operating at $\lambda = 1550$ nm. The power spectral density is calculated from (2-16) and (2-30) as

$$N_{0,\lambda}(T_B) = \frac{2hc^2}{\lambda^3}\frac{1}{e^{hc/\lambda kT_B} - 1}, \tag{2-33}$$

where

$$\Omega_B > \Omega_{FOV}, \tag{2-34}$$

which yields $N_{0,\lambda}(T_B) = (1550\times10^{-9})^2(3.47\times10^{12}) = 8.35$ W/m.

The power spectral density and wavelength relationship is shown in Figure 2. The power spectral density increases as the wavelength decreases for the diffraction-limited case.

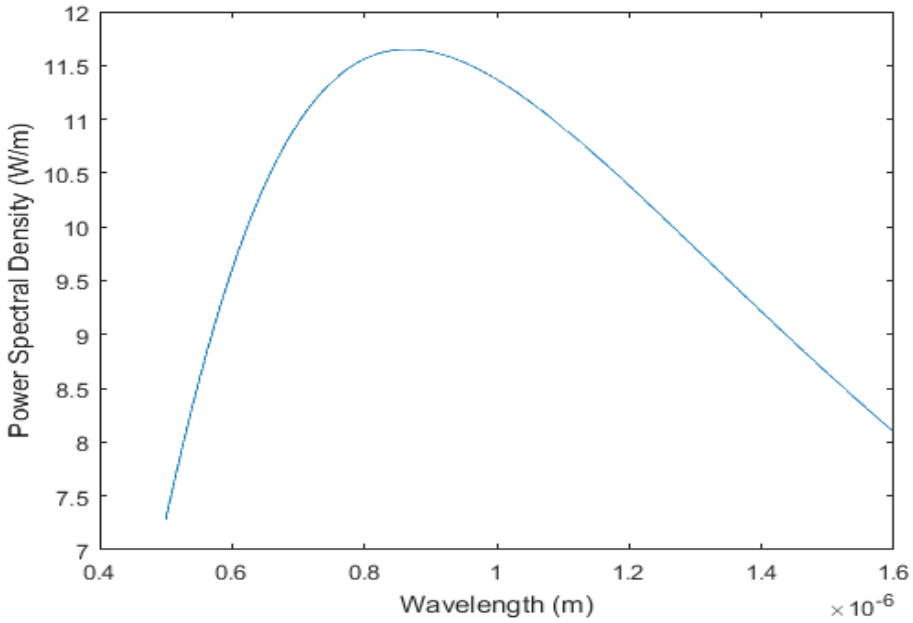

Figure 2. Power Spectral Density of Solar Radiation

Note that the 600 nm wavelength is at the left end of the plot and the 1550 nm wavelength at the right end in Figure 2. This means that 600 nm and 1550 nm wavelengths have the lowest background radiation. For this reason, these wavelengths are most widely used for optical communications.

5. Earth Radiation and Reflected Sunlight

The optical signal that arrives at the receiver may include the Earth's radiation or reflected sunlight for an FSO ground-space communication link. Earth radiation and reflected sunlight decrease the effectiveness of the receiver substantially. Reflected sunlight is the main source of background radiation in most cases. Earth radiation is much less than reflected sunlight by comparison.

Consider the case of an FSO ground-space communication link using an inexpensive laser and a circular lens with wavelength $\lambda = 600$ nm. The ambient light is reflected sunlight, which can be considered as radiation emitted by the Sun at temperature $T_s = 5900$ K. Let α_{ref} be the ratio of the total reflected and incident radiation from the

Earth's surface, which is not an ideal reflector. Note that the reflected and incident radiation pass through the atmosphere [10].

The planar angular of the receiver FOV is $\theta_{FOV} = D_r / d$ for $d \gg D_r$, where the receiver aperture diameter D_r is 0.3 m and d is the distance between the receiver and transmitter. The power spectral density of the reflected sunlight at the received circular lens is calculated as

$$N_{0,\lambda}(\mathrm{T}_B) = \alpha_{ref} \frac{\pi^2 D_r^2}{4d^2} \frac{\pi^2 D_r^2}{4} \frac{2hc^2}{\lambda^5} \frac{1}{e^{hc/\lambda k T_B} - 1}, \tag{2-35}$$

which equals $2.49 \times 10^{10} \alpha_{ref} d^{-2}$ W/m for this case.

For the diffraction-limited case, from (2-33), the power spectral density for reflected sunlight is $9.6\alpha_{ref}$ W/m.

The parameter α_{ref} varies depending on the location and the look angle. The Earth also emits light. Although the intensity is insignificant compared to sunlight, we include both radiation types in our analysis.

It is difficult to determine α_{ref}. We have measured data in Figure 3, which gives the power spectral density for different wavelengths [12].

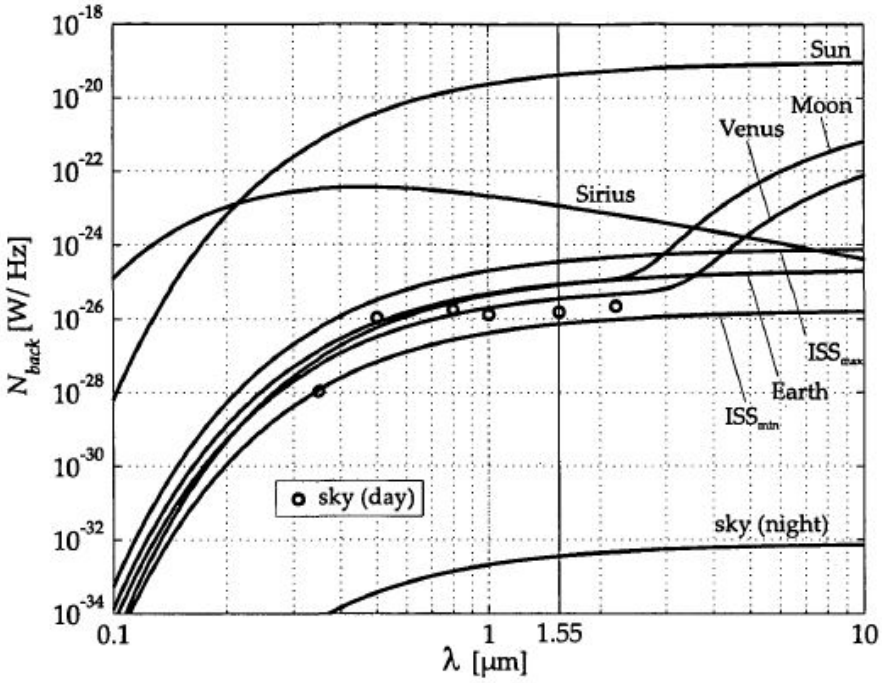

Figure 3. Power Spectral Density (PSD) for Different Celestial Bodies, the Sky during Day and Night by a Diffraction-Limited Telescope. Source: [12].

We determine α_{ref} both for reflected sunlight and Earth radiation using Figure 3. The numbers used to approximate α_{ref} for reflected solar radiation using $T_B = 5900\,\mathrm{K}$ are shown in Table 1. It can be seen that $\alpha_{ref,sun}$ for solar radiation can be approximated to be 0.5 for wavelengths of 600 nm.

The numbers used to approximate $\alpha_{ref,sky}$ for Earth radiation are shown in Table 2 using $T_B = 5400\,\mathrm{K}$, where T_B is the effective temperature for the Earth. The effective temperature is the temperature of the black body that emits the same intensity of radiation as the actual source [13]. We see that $\alpha_{ref,sky}$ for Earth radiation can be approximated as 1.66×10^{-6}.

Table 1. Reference Value Approximation for Solar Radiation, $\alpha_{ref,sun}$. Second column adapted from [12].

Wavelength [nm]	PSD [W/Hz] from Figure 3	Calculated PSD [W/Hz] from (2-30)	Ratio ($\alpha_{ref,sun}$)
1550	4.1×10^{-20}	6.69×10^{-20}	0.61
1000	2×10^{-20}	3.79×10^{-20}	0.52
700	10^{-20}	1.79×10^{-20}	0.55
400	10^{-21}	2.26×10^{-21}	0.44

Table 2. Reference Value Approximation for Earth Radiation, $\alpha_{ref,sky}$. Second column adapted from [12].

Wavelength [nm]	PSD [W/Hz] from Figure 3	Calculated PSD [W/Hz] from (2-30)	Ratio ($\alpha_{ref,sky}$)
1550	8.3×10^{-26}	5.58×10^{-20}	1.48×10^{-6}
1000	6×10^{-26}	2.96×10^{-20}	2×10^{-6}
570	10^{-26}	6.53×10^{-21}	1.5×10^{-6}

We obtain the power spectral density using the approximate $\alpha_{ref,sun}$ with $\lambda = 600$ nm for the diffraction-limited case as

$$N_{0,\lambda,sun}(T_B) = 9.6\alpha_{ref} = 9.6\times 0.5 = 4.8 \text{ W/m.} \quad (2\text{-}36)$$

The Earth's atmosphere attenuates solar radiation substantially; hence, the spectral radiance and the power spectral density are both greatly reduced.

Consider an FSO ground-space communication link operating at a $\lambda = 600$ nm wavelength. The space receiver's optical antenna aperture diameter D_r is 30 cm. The ground transmitter transmits a Gaussian laser beam. The transmit beam divergence angle is $\theta = 0.83$ mrd. The on-axis gain is $G_t = 32/\theta^2 = 76.7$ dB. From (2-10) and (2-11), the received antenna gain is

$$G_r = \left(\frac{\pi D_r}{\lambda}\right)^2 = 123.9 \text{ dB}. \tag{2-37}$$

The divergence diameter of the beam at distance *d* from the transmitter is [9]

$$D_{div} = 2d\tan(\theta/2) \approx d\theta. \tag{2-38}$$

The diameter of the receive antenna D_r captures approximately $(D_r / D_{div})^2$ of the incident power ($1/e^2$ intensity points) [9]:

$$\left(\frac{D_r}{D_{div}}\right)^2 = \left(\frac{D_r}{d\theta}\right)^2 = \left(\frac{0.3}{0.83\times 10^{-3} d}\right)^2 = 13.05\times 10^{-4} d^{-2}. \tag{2-39}$$

From (2-2), the free-space loss is

$$L_{fs} = \left(\frac{4\pi d}{\lambda}\right)^2 = \left(\frac{4\pi}{600\times 10^{-9}}\right)^2 d^2 = 4.387\times 10^{14} d^2. \tag{2-40}$$

From (2-1) and (2-39), the received power is

$$\begin{aligned} P_r &= \frac{P_t G_t G_r \eta_t \eta_r}{L_{fs} L_a L_p}\left(\frac{D_r}{D_{div}}\right)^2 = \frac{P_t (10^{7.67})(10^{12.39})(10^{-0.15})(10^{-0.3})}{4.387\times 10^{14} d^2 L_a L_p} 13.05\times 10^{-4} d^{-2}, \\ &= \frac{121 P_t}{d^4 L_a L_p}. \end{aligned} \tag{2-41}$$

From (2-41), we get the required transmit power as

$$P_t = \frac{P_r d^4 L_a L_p}{121}, \tag{2-42}$$

where the received power-distance product is

$$P_r d^4 = \frac{121 P_t}{L_a L_p}. \tag{2-43}$$

Note that

$$P_r = E_b R_b, \tag{2-44}$$

where E_b is the bit energy and R_b is the bit rate. From (2-42) and (2-44), the bit energy-to-ambient light density ratio is

$$\frac{E_b}{N_{0,f}(T_B)} = \frac{P_r}{R_b N_{0,f}(T_B)} = \frac{121P_t}{R_b d^4 N_{0,f}(T_B) L_a L_p}, \tag{2-45}$$

where $N_{0,f,sun}(T_B)$ is calculated for $\lambda = 600$ nm as [10]

$$N_{0,f,sun}(T_B) = \frac{\lambda^2}{c} N_{0,\lambda,sun}(T_B), \tag{2-46}$$

where $N_{0,\lambda,sun}(T_B)$ is $9.6\alpha_{ref}$ W/m. The power spectral density for reflected sunlight at 600 nm is

$$N_{0,f,sun}(T_B) = \frac{\lambda^2}{c} 9.6\alpha_{ref}, \tag{2-47}$$

which equals 5.76×10^{-21} W/Hz in this case.

Let ρ_{amb} be the required bit energy-to-ambient light density ratio. The following condition must be satisfied:

$$\frac{121P_t}{R_b d^4 N_{0,f}(T_B) L_a L_p} \geq \rho_{amb}. \tag{2-48}$$

Now from (2-48), the upper bound of the bit rate-distance product is given by

$$R_b d^4 \leq \frac{121P_t}{\left\{\max_{f\in B} N_{0,f}(T_B)\right\} \rho_{amb} L_a L_p}. \tag{2-49}$$

Let B be the receiver bandwidth, $R_b < B < 2R_b$. The power spectral density is virtually constant within the bandwidth B for $B \ll f$ (note that B is on the order of GHz and f in THz). Numerically, we get $N_{0,f}(T_B) = 5.76\times10^{-21}$ W/Hz from (2-47).

Let $L_a = 2$ (3 dB), $L_p = 2$ (3 dB), $\rho_{amb} = 25$ (14 dB), and $P_t = 4.2$ W; from (2-49), we obtain

$$R_b d^4 \leq \frac{121\times 4.2}{5.76\times10^{-21}\times 25\times 2\times 2} = 8.82\times10^{20}. \tag{2-50}$$

For $d = 1000$ m, we get $R_b \le 882$ Mb/s at $\lambda = 600$ nm.

Consider the link in the previous example with the wavelength changed to $\lambda = 1550$ nm. The receiver aperture diameter D_r is 30 cm. The transmitter transmits a Gaussian laser beam. The transmit beam divergence is $\theta = 0.83$ mrd. From (2-6) and (2-7), the on-axis gain is $G_t = 32/\theta^2 = 76.7$ dB. From (2-37), the received antenna gain is

$$G_r = \left(\frac{\pi D_r}{\lambda}\right)^2 = 115.7 \text{ dB}. \tag{2-51}$$

From (2-2), the free-space loss is

$$L_{fs} = \left(\frac{4\pi d}{\lambda}\right)^2 = \left(\frac{4\pi}{1550\times 10^{-9}}\right)^2 d^2 = 6.57\times 10^{13} d^2. \tag{2-52}$$

From (2-41), the received power is given by

$$\begin{aligned} P_r &= \frac{P_t G_t G_r \eta_t \eta_r}{L_{fs} L_a L_p}\left(\frac{D_r}{D_{div}}\right)^2 = \frac{P_t (10^{7.67})(10^{11.57})(10^{-0.15})(10^{-0.3})}{6.57\times 10^{13} d^2 L_a L_p} 13.05\times 10^{-4} d^{-2}, \\ &= \frac{122.5 P_t}{d^4 L_a L_p}. \end{aligned} \tag{2-53}$$

From (2-47), the power spectral density of the reflected solar radiation at the received circular lens with $\alpha_{ref,sun} = 0.5$ and $N_{0,\lambda,sun}(T_B) = 9.6\alpha_{ref}$ for $\lambda = 1550$ nm is

$$N_{0,f,sun}(T_B) = \frac{\lambda^2}{c} 9.6\alpha_{ref}, \tag{2-54}$$

which equals 3.34×10^{-20} W/Hz in this case.

Let $L_a = 2$ (3 dB), $L_p = 2$ (3 dB), $\rho_{amb} = 25$ (14 dB), and $P_t = 4.2$ W; from (2-49), we obtain

$$R_b d^4 \le \frac{122.5\times 4.2}{3.34\times 10^{-20}\times 25\times 2\times 2} = 1.41\times 10^{20}. \tag{2-55}$$

For $d = 1000$ m, we get $R_b \le 141$ Mb/s at $\lambda = 1550$ nm.

The FSO communication link bit rate and distance relation to reflected solar radiation is shown in Figure 4 for both $\lambda = 600$-nm and $\lambda = 1550$-nm wavelengths. As can be seen from Figure 4, the bit rate increases as the distance decreases, and the

difference between wavelengths is also observed. When the wavelength is 600 nm, the FSO communication link is available for greater distances.

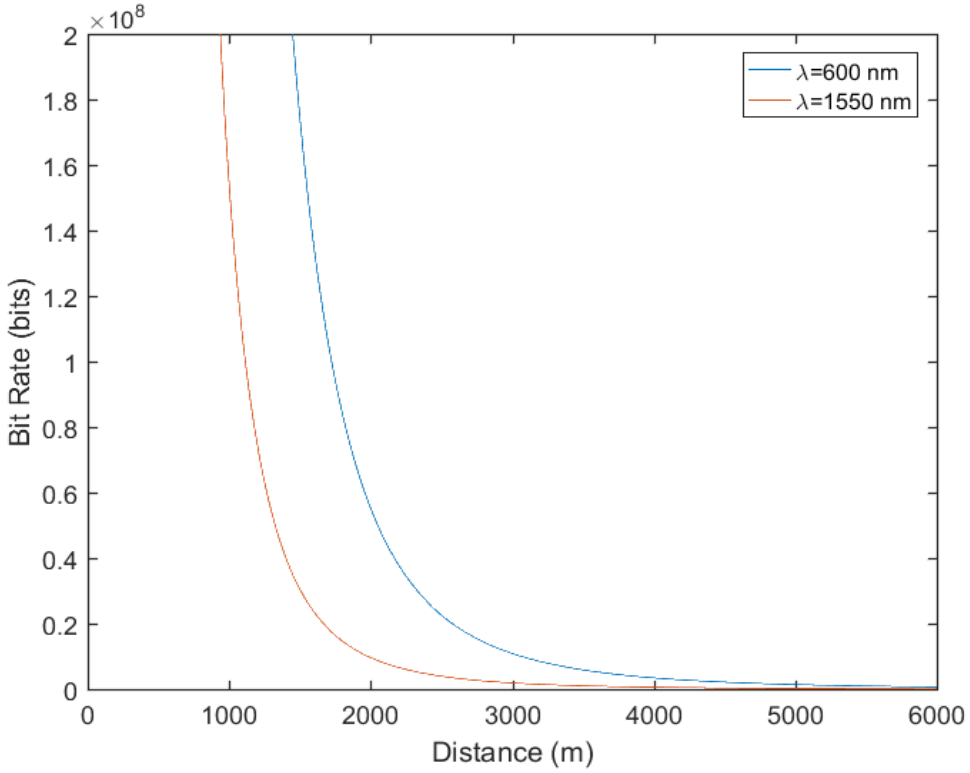

Figure 4. FSO Communication Link Bit Rate and Distance with Reflected Solar Radiation at $\lambda = 600$ nm and $\lambda = 1550$ nm

The bit rate decreases substantially for a distance greater than 4.0 km for $\lambda = 600$ nm and 3.0 km for $\lambda = 1550$ nm. Establishing communications is still possible but the data rate is slow.

Note that the 600 nm wavelength optical signal is visible to the human eye and is considered harmful to the human eye and skin when used at high power. Since low-power lasers are used in our link analysis, there is no obstacle to use the 600-nm wavelength optical signal.

B. CONCLUSION

The analysis above does not include the receiver noise (photo detection's shot noise and amplifier noise), which is estimated to be on the same order of magnitude as the background noise. If error correction coding is introduced, coding gain is expected to range from 4 dB to 6 dB, which will compensate for receiver noise. For a goal of 10^{-9} bit error probability, the required bit energy-to-noise density ratio is approximately 14 dB.

The most plausible approach to increase the bit-rate distance product is to use lasers that have smaller beam divergence angles. Consider the FSO system example with $\lambda = 600$ nm, assume the bit rate remains constant, and the laser beam divergence angle is reduced from 0.83 mrd to 0.415 mrd, then received power increases and the distance between the transmitter and receiver can be increased from 1.0 km to 2.3 km. If a laser with 0.1 mrd is used, the distance can be further increased to 9.0 km.

Higher bit rate and longer distances require antenna optics. Intensity modulation/direct detection (IM/DD) is the most preferable method for inexpensive lasers. IM/DD can be used very effectively for shorter distances. Homodyne or heterodyne receivers with phase modulation such as phase-shift keying (PSK), quadrature phase-shift keying (QPSK), and orthogonal-frequency division multiplexing (OFDM) are superior in performance if antenna optics are used. Inexpensive lasers may have high phase noise and can substantially reduce the performance of coherent receivers to the level of direct- detection receivers, which are much cheaper to build.

THIS PAGE INTENTIONALLY LEFT BLANK

III. MODULATION AND DEMODULATION

A. OPTICAL MODULATION

There are many types of modulation used in optical communications. These include On-Off keying, phase-shift keying, pulse-amplitude modulation, pulse-width modulation, pulse-position modulation and variations like differential PPM (DPMM) and *M*-ary PPM. In this chapter, *M*-ary PPM with a novel method of direct detection is examined because of its power efficiency for optical communications. Later, *M*-ary PPM is compared with OOK.

B. *M*-ARY PPM INTENSITY MODULATION

Pulse-position modulation is a type of digital pulse modulation. In this modulation, the message signal modulates the positions of a carrier signal in each time slot *T*. *M*-ary PPM consists of *M* symbols within each time slot *T*. The symbol time is T_s where $T_s = MT$. Each symbol consists of n bits, $M = 2^n$, or $n = \log_2 M$. Each PPM signal has exactly one pulse in a designated time slot. An *M*-ary PPM waveform can be expressed as

$$s_i(t),\ i = 0,1,...,M-1;\ 0 \le t \le T_s, \tag{3-1}$$

where $s_i(t)$ is a pulse in the i-th time slot. The remaining $M-1$ time slots ideally have no pulses. In practice, the light source does not turn off completely, so there is some residual light in the $M-1$ supposedly empty slots.

The PPM intensity modulator block diagram is shown in Figure 5. The message bits are mapped to their assigned symbols; afterwards, the PPM waveform generator creates PPM pulses, and the optical light source emits different intensities of light determined by the modulated PPM signal.

The PPM waveform for the i-th symbol can be derived from OOK modulation waveform as [14]

$$s_i(t) = \begin{cases} \frac{1}{\sqrt{1+r_e}} Ap(t-iT)\cos(2\pi f_c t): \text{ on} \\ \sqrt{\frac{r_e}{1+r_e}} Ap(t-kT)\cos(2\pi f_c t), k \neq i, k = 0,1,...,M-1: \text{ off} \end{cases}, \quad (3\text{-}2)$$

where r_e is called the extinction ratio, which is the ratio of the light energy for bit 0 to that for bit 1 and is within the range of 0 and 1 [14], *A* is the carrier amplitude, $p(t)$ is the squared pulse of unit amplitude, *T* is the duration of the pulse, and f_c is the carrier frequency.

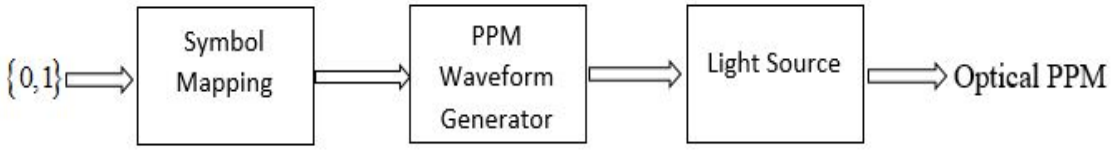

Figure 5. PPM Intensity Modulator

Symbol-pulse positions for each 4-PPM symbol are shown in Figure 6. In this case, each symbol time T_s is divided into four equal time slots. Bold lines represent the times when the light source is supposedly off.

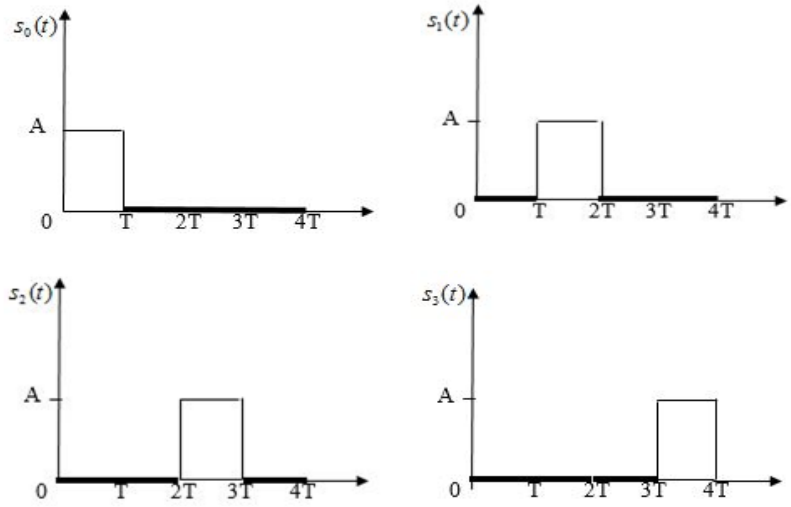

Figure 6. 4-PPM Symbol-Pulse Positions

Bits-to-symbol mapping for 4-PPM is shown in Table 3. Every symbol has two bits in the case of 4-PPM. This mapping can be extended to 8-PPM and 16-PPM, where three bits and four bits, respectively, are transmitted on each symbol.

Table 3. Bits-to-Symbol Mapping for 4-PPM

Symbol	Bits	Time Slot
$s_0(t)$	00	$0 \le t \le T$
$s_1(t)$	01	$T \le t \le 2T$
$s_2(t)$	11	$2T \le t \le 3T$
$s_3(t)$	10	$3T \le t \le 4T$

When the optical signal is received, the receiver decides during which time slot the high pulse is received and maps symbols back to bits.

The *M*-ary PPM symbol energy *E* can be written as

$$E = \int_0^{T_s} s_i^2(t)dt = \int_0^{T_s} s_1^2(t)dt. \tag{3-3}$$

Substituting (3-2) into (3-3), we get

$$E = \int_0^{T} \left(\frac{1}{\sqrt{1+r_e}} A\cos(2\pi f_c t) \right)^2 dt + \int_T^{MT} \left(\sqrt{\frac{r_e}{1+r_e}} A\cos(2\pi f_c t) \right)^2 dt. \tag{3-4}$$

Using the integration calculation for symbol energy in [14], we get the *M*-ary PPM symbol energy as

$$\begin{aligned} E &= \frac{A^2T}{2}\left(\frac{1}{1+r_e}\right) + \frac{A^2T(M-1)}{2}\left(\frac{r_e}{1+r_e}\right) = \frac{A^2T}{2(1+r_e)} + \frac{A^2T(M-1)r_e}{2(1+r_e)}, \\ E &= \frac{A^2T}{2}\left(\frac{1+(M-1)r_e}{1+r_e}\right). \end{aligned} \tag{3-5}$$

If $r_e = 0$ then, *M*-ary PPM symbol energy reduces to

$$E = \frac{A^2 T}{2}. \tag{3-6}$$

Since *M*-ary PPM has a 1/*M* duty cycle, the average energy E_p of the on-pulse and off-pulse can be expressed as

$$E_p = \begin{cases} \frac{1}{M}\int_0^T \left(\frac{1}{\sqrt{1+r_e}} A\cos(2\pi f_c t) \right)^2 dt = \frac{A^2 T}{2M(1+r_e)} : \text{ on} \\ \frac{1}{M}\int_T^{2T} \left(\sqrt{\frac{r_e}{1+r_e}} A\cos(2\pi f_c t) \right)^2 dt = \frac{A^2 T r_e}{2M(1+r_e)} : \text{ off} \end{cases}. \tag{3-7}$$

The *M*-ary PPM signal-space waveform can be expressed as

$$s_i(t) = \left[\frac{1}{\sqrt{1+r_e}} Ap(t-iT) + \sum_{\substack{k=0 \\ k\neq i}}^{M-1} \sqrt{\frac{r_e}{1+r_e}} Ap(t-kT) \right] \cos(2\pi f_c t). \tag{3-8}$$

Power spectral density $S(f)$ of *M*-ary PPM is given by [15]

$$S(f) = |P(f)|^2 \left[S_c(f) + S_d(f) \right], \tag{3-9}$$

where S_c and S_d are the continuous and discrete parts of the signal, respectively, and are expressed as [15]

$$S_c(f) = \frac{1}{T}\left[\left(1 - \frac{1}{M} \right) + \frac{2}{M} \sum_{k=1}^{M-1} \left(\frac{k}{M} - 1 \right) \cos\left(\frac{k 2\pi f T}{M} \right) \right], \tag{3-10}$$

$$S_d(f) = \frac{2\pi}{T^2} \sum_{k=-\infty}^{\infty} \delta\left(f - \frac{kM}{T} \right). \tag{3-11}$$

The power spectral density of *M*-ary PPM is shown in Figure 7. We see that as *M* increases, both bandwidth and transmitted power increase. If the bandwidth requirement is not critical, *M*-ary PPM is a better choice for optical communications in terms of power efficiency for large *M*.

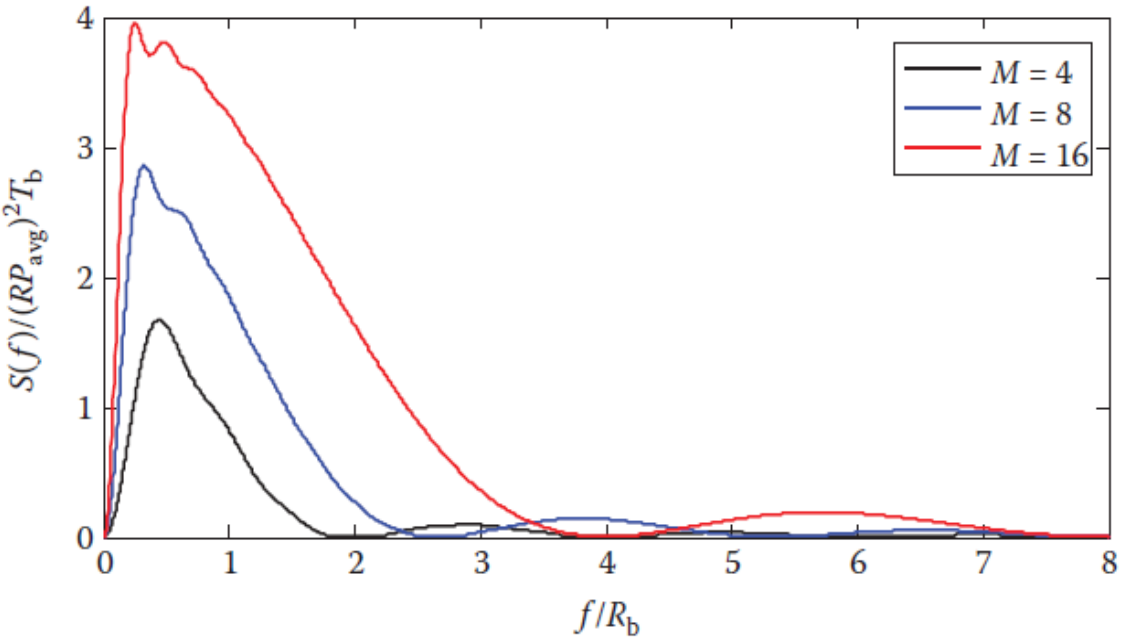

Figure 7. Power Spectral Density of *M*-ary PPM for $M = 4$, 8, and 16. Adapted from [16].

C. OPTICAL DEMODULATION

Optical demodulation consists of direct, homodyne, and heterodyne detection techniques. Direct detection is also a baseband demodulation method [10]. A novel method of direct detection of *M*-ary PPM is investigated here because of its efficiency and simplicity.

D. DIRECT DETECTION OF *M*-ARY PPM

One of the significant characteristics of direct detection is that, unlike other detection methods, it does not use a laser oscillator while demodulating the optical signal. Direct detection is commonly used with intensity modulation [16]. A block diagram for direct detection is shown in Figure 8.

Since *M*-ary PPM intensity modulation consists of different positions of on-off signals, using direct detection for demodulation is a wise choice.

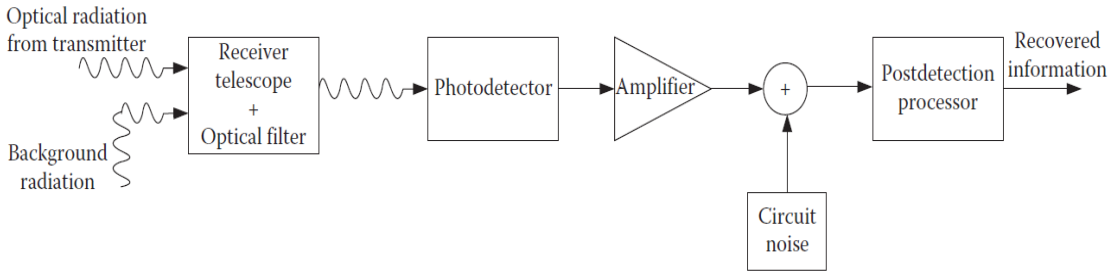

Figure 8. Direct Detection. Source: [16].

Direct detection of *M*-ary PPM is illustrated in Figure 9. The *M*-ary PPM signal is detected by a photo detector with a current output and amplified by a transimpedance amplifier. This amplification is required because background radiation causes the photo detector to generate shot noise.

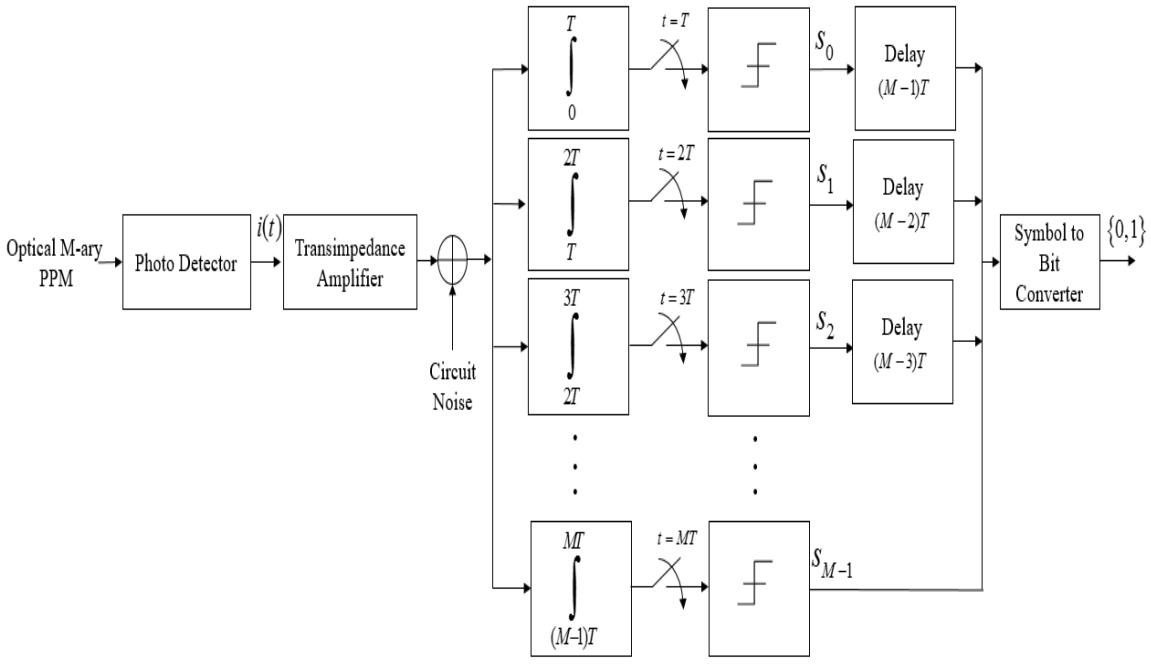

Figure 9. *M*-ary PPM Demodulation

To decrease the effects of shot noise, preamplification is applied to the output of the photo detector [16]. In the amplification process, circuit noise is added to the signal (thermal noise generated by the amplifier). The voltage signal is applied to the integrator,

which yields the energy of the signal as output. The signal is delayed to provide the correct order of *M*-ary PPM pulses to the threshold detector. The threshold detector determines whether the signal level is over the threshold voltage. If it is over the threshold voltage, the symbol corresponds to the branch that detects the pulse is declared. This process is repeated for every symbol time T_s. This means that only one symbol is declared every T_s s even the detection is accomplished within a time slot *T*. Finally, the symbol-to-bit converter maps the symbols to bits.

Symbol-to-bits mapping for 4-PPM is shown in Table 4. The demodulator generates one symbol consisting of four chips every symbol time T_s. We clearly see that *M*-ary PPM increases the bandwidth but also increases the number of bits delivered compared with OOK. This relationship is given by [16]

$$T = \frac{nT_{b,OOK}}{M}, \tag{3-12}$$

where $T_{b,OOK}$ is bit duration of OOK and n is the number of bits. This means that *M*-ary PPM pulse durations are *M*/*n* times shorter than OOK pulse (or bit) durations.

Table 4. Symbol-to-Bits Mapping for 4-PPM

Threshold Detector Output Chips of A Symbol	Symbol Signal	Bits	Time Slot
1000	$s_0(t)$	00	$0 \le t \le T$
0100	$s_1(t)$	01	$T \le t \le 2T$
0010	$s_2(t)$	11	$2T \le t \le 3T$
0001	$s_3(t)$	10	$3T \le t \le 4T$

The photo detector receives the optical signal $s_i(t)$ and generates a current as output. The output current $i(t)$ of a photo detector for the *i*-th symbol can be expressed as [14]

$$i(t)=\begin{cases}\dfrac{\Re A^2}{2(1+r_e)}\,p(t-iT)+i_s(t):\ \text{on}\\ \dfrac{\Re A^2}{2}\left(\dfrac{r_e}{1+r_e}\right)p(t-kT)+i_s(t),k\neq i,k=0,1,...,M-1:\ \text{off}\end{cases}, \tag{3-13}$$

where $\Re$ is the responsivity of the photo detector and i_s is the shot-noise current generated by photo detector. The performance of photo detector is defined by its responsivity. Responsivity is 0.7 A/W for wavelengths of 1300 and 1500 nm [14].

The output voltage of the transimpedance amplifier is given by [14]

$$x(t)=Z_0\left[i(t)+i_a(t)\right], \tag{3-14}$$

where Z_0 is the impedance and $i_a(t)$ is the internal noise current of the amplifier. Using (3-13), we get the output voltage of the transimpedance amplifier $x(t)$ corresponding to the transmitted optical signal $s_i(t)$ for the *i*-th symbol as

$$x(t)=\begin{cases}\dfrac{Z_0\Re A^2}{2(1+r_e)}\,p(t-iT)+Z_0i_n(t):\ \text{on}\\ \dfrac{Z_0\Re A^2}{2}\left(\dfrac{r_e}{1+r_e}\right)p(t-kT)+Z_0i_n(t),k\neq i,k=0,1,...,M-1:\ \text{off}\end{cases}, \tag{3-15}$$

where

$$i_n(t)=i_s(t)+i_a(t) \tag{3-16}$$

is the total noise current with power spectral density N_0 (A^2/Hz). In practice, $i_a(t)\gg i_s(t)$, and the signal $x(t)$ is integrated by integrators for one pulse time *T*. The output of the integrators and input to the threshold detectors is

$$X=\begin{cases}X_i=\dfrac{Z_0\Re A^2T}{2(1+r_e)}+N:\ H_i\\ X_k=\dfrac{Z_0\Re A^2T}{2}\left(\dfrac{r_e}{1+r_e}\right)+N,k\neq i,k=0,1,...,i-1:\ H_k\end{cases}, \tag{3-17}$$

where

$$N = \int_0^T Z_0 i_n(t)dt, \tag{3-18}$$

is the integrated noise, which can be modeled as additive white Gaussian noise (AWGN) with zero mean; H_i is the hypothesis when received pulse is greater than the threshold voltage, and H_k is the hypothesis when the received pulse is less than the threshold voltage.

The noise voltage $Z_0 i_n(t)$ is modeled as AWGN with zero mean and power spectrum

$$S_{Z_0, i_n(t)}(f) = Z_0^2 N_0. \tag{3-19}$$

The variance is

$$\sigma^2 = E\left\{N^2\right\} = Z_0^2 N_0 T. \tag{3-20}$$

The *M*-ary PPM received average power $P_{ave,PPM}$ can be expressed using (3-5) as

$$\begin{aligned} P_{ave,PPM} &= \frac{E}{T_s} = \frac{E}{MT} = \frac{A^2}{2M(1+r_e)} + \frac{A^2(M-1)r_e}{2M(1+r_e)}, \\ &= \frac{A^2(1+(M-1)r_e)}{2M(1+r_e)}. \end{aligned} \tag{3-21}$$

If $r_e = 0$, the average power can be reduced to

$$P_{ave,PPM} = \frac{A^2}{2M}. \tag{3-22}$$

The threshold detector detects a pulse that has a voltage larger than the threshold voltage V_T. The probability of pulse error for threshold detection is given by [14]

$$p = Q\left(\frac{m_1 - m_2}{2\sigma}\right), \tag{3-23}$$

where m_1 is the mean value for hypothesis H_i when it is over the threshold voltage and m_2 is mean value for hypothesis H_k when it is below the threshold voltage. The means m_1 and m_2 can be expressed using (3-17) as

$$
\begin{aligned}
m_1 &= E\left\{X \middle| H_i\right\} = \frac{Z_0 \Re A^2 T}{2(1+r_e)}, \\
m_1 &= E\left\{X \middle| H_k\right\} = \frac{Z_0 \Re A^2 T}{2}\left(\frac{r_e}{1+r_e}\right), k \neq i, k = 0,1,...,i-1.
\end{aligned}
\tag{3-24}
$$

Substituting (3-24) and (3-20) into (3-23), we get the probability of pulse error in time slot T as

$$
\begin{aligned}
p &= Q\left(\frac{\frac{Z_0 \Re A^2 T}{2(1+r_e)} - \frac{Z_0 \Re A^2 T}{2}\left(\frac{r_e}{1+r_e}\right)}{2\sqrt{Z_0^2 N_0 T}}\right), \\
&= Q\left(\frac{\frac{Z_0 \Re A^2 T(1-r_e)}{2(1+r_e)}}{2Z_0\sqrt{N_0 T}}\right) = Q\left(\frac{Z_0 \Re A^2 T(1-r_e)}{4Z_0\sqrt{N_0 T}(1+r_e)}\right), \\
&= Q\left(\frac{\Re A^2(1-r_e)}{4(1+r_e)}\sqrt{\frac{T}{N_0}}\right).
\end{aligned}
\tag{3-25}
$$

Using the M-ary PPM average received power $P_{ave,PPM}$ given in (3-22), we get the probability of pulse error in terms of power as

$$
p = Q\left(\frac{\Re P_{ave,PPM} M(1-r_e)}{2(1+r_e)}\sqrt{\frac{T}{N_0}}\right). \tag{3-26}
$$

If $r_e = 0$, (3-26) becomes

$$
p = Q\left(\frac{\Re P_{ave,PPM} M}{2}\sqrt{\frac{T}{N_0}}\right). \tag{3-27}
$$

The probability of detection of a pulse P_{dp} can be expressed as

$$
\begin{aligned}
P_{dp} &= 1 - p, \\
&= 1 - Q\left(\frac{\Re P_{ave,PPM} M}{2}\sqrt{\frac{T}{N_0}}\right), i = 1,2,...,M.
\end{aligned}
\tag{3-28}
$$

The symbol-detection probability can be obtained via the following reasoning:

a) Assume hypothesis H_0 (symbol signal $s_0(t)$ is transmitted); if the threshold detector 0 of branch 0 detects a pulse (first time slot), the detection probability of symbol 1 is $1-p$. The threshold detector 0 waits for an additional $(M-1)T$ seconds (or $M-1$ time slots) to declare the first symbol of the symbol-set to the symbol-to-bit converter.

b) Assume hypothesis H_1 (symbol signal $s_1(t)$ is transmitted); if the threshold detector 0 of branch 0 detects no pulse (first time slot) and the threshold detector 1 of branch 1 detects a pulse (second time slot), then the detection probability of symbol 2 is the joint detection of no pulse in branch 0 and a pulse in branch 1, which is $(1-p)(1-p)=(1-p)^2$. The threshold detector 1 waits for an additional $(M-2)T$ seconds (or $M-2$ time slots) to declare the second symbol of the symbol-set to the symbol-to-bit converter.

If we generalize this concept, the probability of detection for every symbol can be written as

$$P_{d|H_i}=(1-p)^{i+1}, i=0,1,...,M-1=\begin{cases} P_{d|H_0}=(1-p) \\ P_{d|H_1}=(1-p)^2 \\ \bullet \\ \bullet \\ \bullet \\ P_{d|H_{M-1}}=(1-p)^M \end{cases}, \tag{3-29}$$

where $P_{d|H_i}$ is the probability of detection for hypothesis H_i when the *i*-th pulse is transmitted. Since the probability of H_i is 1/*M*, using the total probability theorem, the *M*-ary PPM probability of detection P_d is calculated from

$$\begin{aligned} P_d &= \frac{1}{M}P_{d|H_0}+\frac{1}{M}P_{d|H_1}+\frac{1}{M}P_{d|H_2}+\cdots+\frac{1}{M}P_{d|H_{M-1}}, \\ P_d &= \frac{1}{M}\sum_{i=0}^{M-1}P_{d|H_i}. \end{aligned} \tag{3-30}$$

Substituting (3-29) into (3-30), we get

$$P_d = \frac{1}{M}\sum_{i=0}^{M-1}(1-p)^{i+1}. \tag{3-31}$$

Let $l = i+1$; now

$$P_d = \frac{1}{M}\sum_{l=1}^{M}(1-p)^{l}. \tag{3-32}$$

In practice, if $p \ll 1$ ($p < 10^{-6}$ for optical communication), $(1-p)^l \approx (1-lp)$, and we obtain the probability of symbol detection for *M*-ary PPM as

$$\begin{aligned} P_d &\approx \frac{1}{M}\sum_{l=1}^{M}(1-lp), \\ &\approx \frac{1}{M}\left[\sum_{l=1}^{M}(1)-\sum_{l=1}^{M}(lp)\right], \\ &\approx \frac{1}{M}\left[M - p\sum_{l=1}^{M} l\right], \\ &\approx \frac{1}{M}\left[M - p\frac{M(M+1)}{2}\right], \\ &\approx 1 - p\frac{M(M+1)}{2M}, \\ &\approx 1 - p\frac{(M+1)}{2}. \end{aligned} \tag{3-33}$$

Using (3-33), we can derive the probability of symbol error P_e for *M*-ary PPM from

$$\begin{aligned} P_e &= 1 - P_d, \\ &= 1 - \left[1 - p\frac{(M+1)}{2}\right], \\ &= \frac{p(M+1)}{2}. \end{aligned} \tag{3-34}$$

Substituting (3-26) into (3-34) yields

$$P_e = \frac{(M+1)}{2} Q\left(\frac{\Re P_{ave,PPM} M(1-r_e)}{2(1+r_e)}\sqrt{\frac{T}{N_0}}\right). \tag{3-35}$$

The probability of symbol error to probability of bit error conversion is given by [14]

$$P_b = \frac{M/2}{M-1} P_e. \tag{3-36}$$

Using (3-35) and (3-36), we obtain the probability of bit error for *M*-ary PPM $P_{b,PPM}$ as

$$\begin{aligned} P_{b,PPM} &= \frac{(M+1)}{2} \frac{M/2}{(M-1)} Q\left(\frac{\Re P_{ave,PPM} M(1-r_e)}{2(1+r_e)} \sqrt{\frac{T}{N_0}} \right), \\ &= \frac{M(M+1)}{4(M-1)} Q\left(\frac{\Re P_{ave,PPM} M(1-r_e)}{2(1+r_e)} \sqrt{\frac{T}{N_0}} \right). \end{aligned} \tag{3-37}$$

The probability of bit error for OOK modulation is given by [14]

$$P_{b,OOK} = Q\left(\frac{\Re P_{ave,OOK}(1-r_e)}{(1+r_e)} \sqrt{\frac{T_{b,OOK}}{N_0}} \right), \tag{3-38}$$

where $P_{ave,OOK}$ is average power of OOK signal and is defined by [14]

$$P_{ave,OOK} = \frac{A^2}{4}, \tag{3-39}$$

where $T_{b,OOK}$ is the bit duration for OOK modulation. The *M*-ary PPM slot time T can be compared with the OOK modulation bit duration $T_{b,OOK}$ as

$$\begin{aligned} T_{b,OOK} &= \frac{T_s}{\log_2 M} = \frac{MT}{\log_2 M}, \\ T &= \frac{T_{b,OOK} \log_2 M}{M}. \end{aligned} \tag{3-40}$$

The probability of bit error for *M*-ary PPM in terms of $T_{b,OOK}$ can be expressed using (3-40) as

$$P_{b,PPM} = \frac{M(M+1)}{4(M-1)} Q\left(\frac{\Re P_{ave,PPM} M(1-r_e)}{2(1+r_e)} \sqrt{\frac{T_{b,OOK} \log_2 M}{MN_0}} \right). \tag{3-41}$$

Using (3-38) and (3-41), we obtain the relationship between the average power for *M*-ary PPM $P_{ave,PPM}$ and the average power for OOK modulation $P_{ave,OOK}$ as

$$\frac{P_{b,OOK}}{P_{b,PPM}} = \frac{Q\left(\frac{\Re P_{ave,OOK}(1-r_e)}{(1+r_e)}\sqrt{\frac{T_{b,OOK}}{N_0}}\right)}{\frac{M(M+1)}{4(M-1)}Q\left(\frac{\Re P_{ave,PPM}M(1-r_e)}{2(1+r_e)}\sqrt{\frac{T_{b,OOK}\log_2 M}{MN_0}}\right)}. \tag{3-42}$$

Using the inverse Q-function, we get

$$\frac{Q^{-1}\left(P_{b,OOK}\right)}{Q^{-1}\left(\frac{4(M-1)P_{b,PPM}}{M(M+1)}\right)} = \frac{\frac{\Re P_{ave,OOK}(1-r_e)}{(1+r_e)}\sqrt{\frac{T_{b,OOK}}{N_0}}}{\frac{\Re P_{ave,PPM}M(1-r_e)}{2(1+r_e)}\sqrt{\frac{T_{b,OOK}\log_2 M}{MN_0}}}, \tag{3-43}$$

which can be manipulated to obtain

$$\frac{Q^{-1}\left(P_{b,OOK}\right)}{Q^{-1}\left(\frac{4(M-1)P_{b,PPM}}{M(M+1)}\right)} = \frac{2P_{ave,OOK}}{P_{ave,PPM}}\sqrt{\frac{1}{M\log_2 M}}. \tag{3-44}$$

Finally, from (3-44), we get

$$P_{ave,PPM} = P_{ave,OOK}\frac{2}{\sqrt{M\log_2 M}}\frac{Q^{-1}\left(\frac{4(M-1)P_{b,PPM}}{M(M+1)}\right)}{Q^{-1}\left(P_{b,OOK}\right)}. \tag{3-45}$$

Assume $P_{b,PPM} = P_{b,OOK} = 10^{-6}$ and $M = 4$; the relationship between the average power for *M*-ary PPM $P_{ave,PPM}$ and the average power for OOK modulation $P_{ave,OOK}$ is, from (3-45),

$$P_{ave,PPM} = 0.725P_{ave,OOK}. \tag{3-46}$$

This means that 4-PPM has a 1.4 dB advantage over OOK modulation. Assume $M = 8$; the relationship between the average power for *M*-ary PPM $P_{ave,PPM}$ and average power for OOK modulation $P_{ave,OOK}$ is, from (3-45),

$$P_{ave,PPM} = 0.428P_{ave,OOK}. \tag{3-47}$$

This means that 8-PPM has a 3.7 dB advantage over OOK modulation. Assume $M = 16$; the relationship between the average power for *M*-ary PPM $P_{ave,PPM}$ and the average power for OOK modulation $P_{ave,OOK}$ is, from (3-45),

$$P_{ave,PPM} = 0.269 P_{ave,OOK}. \tag{3-48}$$

This means that 16-PPM has a 5.7 dB advantage over OOK modulation.

Let β be the power ratio of the average power of *M*-ary PPM and OOK, which is defined as $\beta = P_{ave,PPM} / P_{ave,OOK}$. The probability of bit error versus β for different *M* is shown in Figure 10. It can be clearly seen that as the *M* increases, the power requirement for the *M*-ary PPM signal decreases. This confirms that *M*-ary PPM is much more power efficient than OOK.

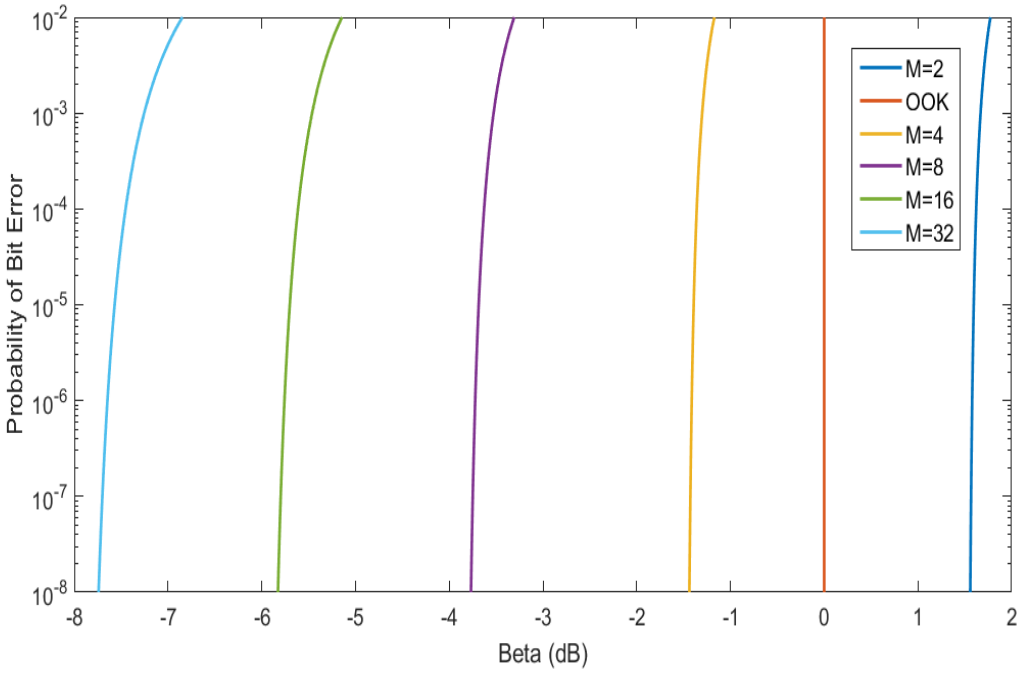

Figure 10. *M*-ary PPM and OOK Power Requirement Ratio Comparison

Consider a direct detection of *M*-ary PPM with total noise spectrum $N = 10^{-22}$ A^2/Hz. The photo detector has a responsivity of $\Re = 0.7$ A/W. The received

M-ary PPM signal has an extinction ratio of $r_e = 0.1$. The bit duration of the signal $T_{b,PPM}$ is 100 μs. The *M*-ary PPM and OOK modulation signal power requirement versus bit error ratio is shown in Figure 11. The results we get are similar to those shown in Figure 10. Note that 32-PPM has 7.6 dB power advantage over OOK modulation at $P_b = 10^{-6}$.

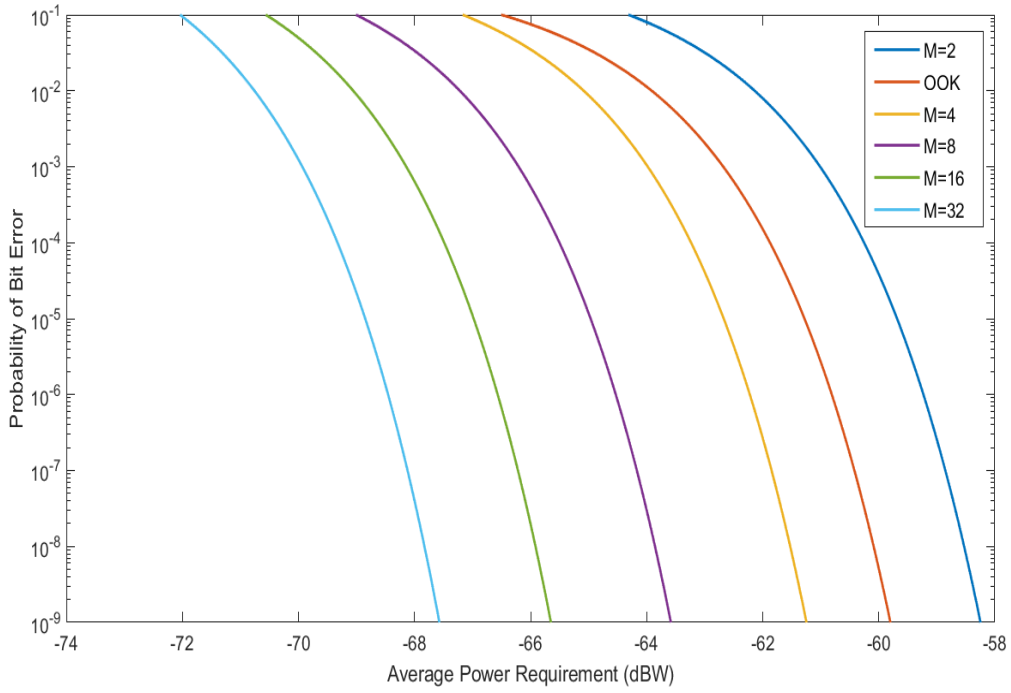

Figure 11. *M*-ary PPM and OOK Modulation Power Requirement Comparison

E. CONCLUSION

In this chapter, the *M*-ary PPM intensity modulation and demodulation process with a novel method of direct detection were explained, and their specific equations for probability of pulse error, probability of detection, probability of symbol error, and probability of bit error were derived. *M*-ary PPM was compared with OOK.

The results obtained confirm that *M*-ary PPM is more power efficient than OOK. Considering that the bandwidth increase for optical communications is not an issue, using *M*-ary PPM with inexpensive lasers is the preferred method.

IV. SIMULATION

Designing a simulation for optical communications is not different from designing a simulation for RF communications. The Simulink tool in Matlab can be used for this purpose. In this chapter, a simulation for *M*-ary PPM with direct detection is designed using Simulink. A performance analysis for the simulation is then presented, comparing the power efficiency of *M*-ary PPM to OOK. We intend to confirm the analytical results presented in Chapter III with this simulation.

A. SIMULATION OF *M*-ARY PPM IN SIMULINK

A block diagram of an *M*-ary PPM modulator is shown in Figure 12, where *M* random integers are provided to the modulator block every *T* seconds to generate random *M*-ary PPM pulses.

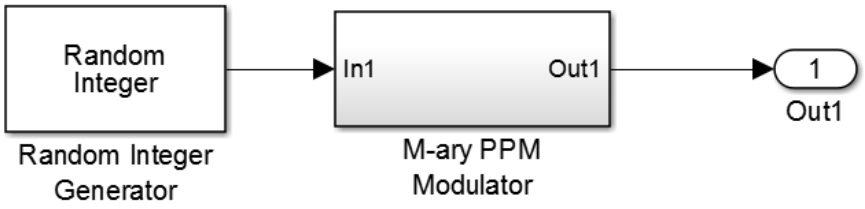

Figure 12. *M*-ary PPM Modulator

M-ary PPM is a combination of *T* time delays of *M* pulses. To generate delayed pulses in Simulink, every pulse transmitted by the pulse generator is delayed using a delay block; however, using delay blocks converts sampling-based pulses to continuous-time based pulses and causes problems for bit error ratio (BER) calculations. Instead, we use *M* pulse generators.

The *M*-ary PPM modulator block for 4-PPM is shown in Figure 13. Random integers are provided to the modulator from port in1. Pulse generator 1 generates four pulses every *T* seconds without delay. Pulse generator 2 generates the same pulse as pulse generator 1, but the pulse is delayed one pulse time *T*. The delay value for pulse generator 2 is set to one sample time, which is the slot time *T*. Pulse generator 3 delays the signal

two pulse times 2*T*. Pulse generator 4 delays the signal three pulse times 3*T*. Outputs of the pulse generators are connected to a multiport switch. The multiport switch receives random integers from its first port. Depending on the received integer number, it transmits one symbol from one of its ports for a duration of 4*T* seconds. Note that the random integer generator generates the same integer for the duration of 4*T* seconds, which allows the multiport switch to let through a complete symbol pulse.

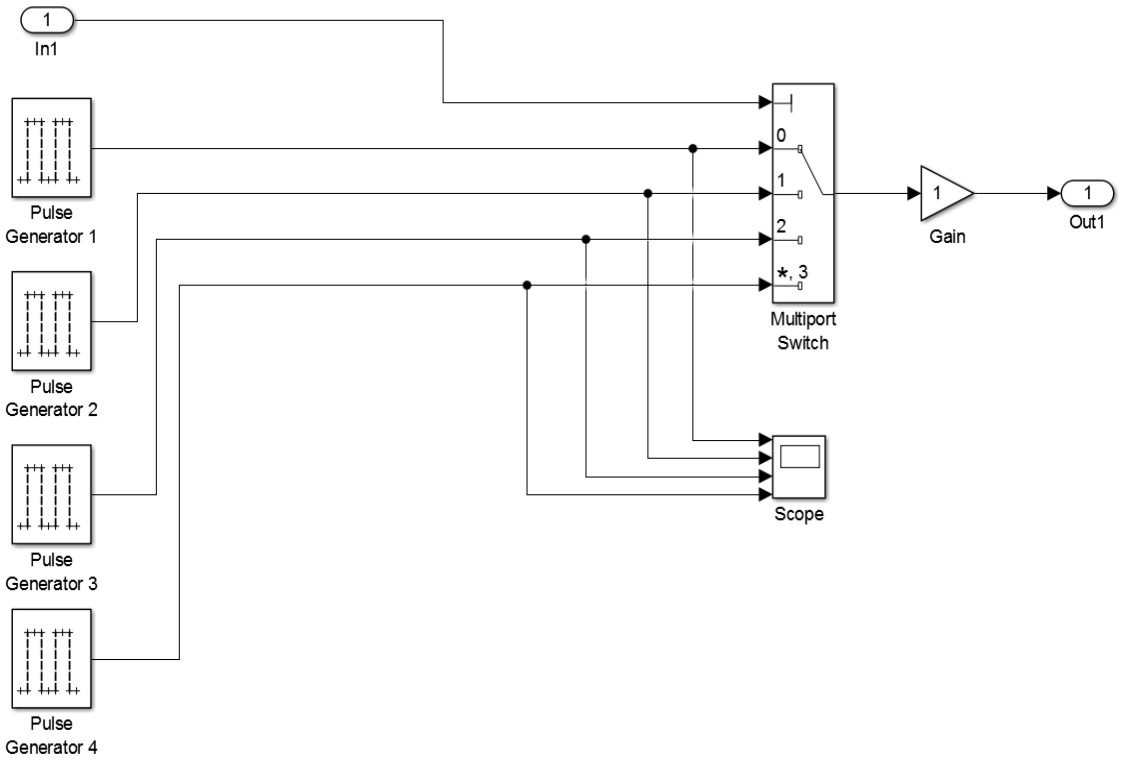

Figure 13. 4-PPM Modulator Block

The output of the multiport switch is provided to the gain block. Signal amplitude *A* is set to 1.0 by this gain block. The signal is then sent to the demodulator from the Out1 port. Note that this simulation was designed in baseband for simulation purposes, which means that pulses are not modulated by a sine wave. Signal pulses generated by every pulse generator are shown in Figure 14. The pulse generators generate the same pulse for every symbol time T_s, or every 4*T* seconds.

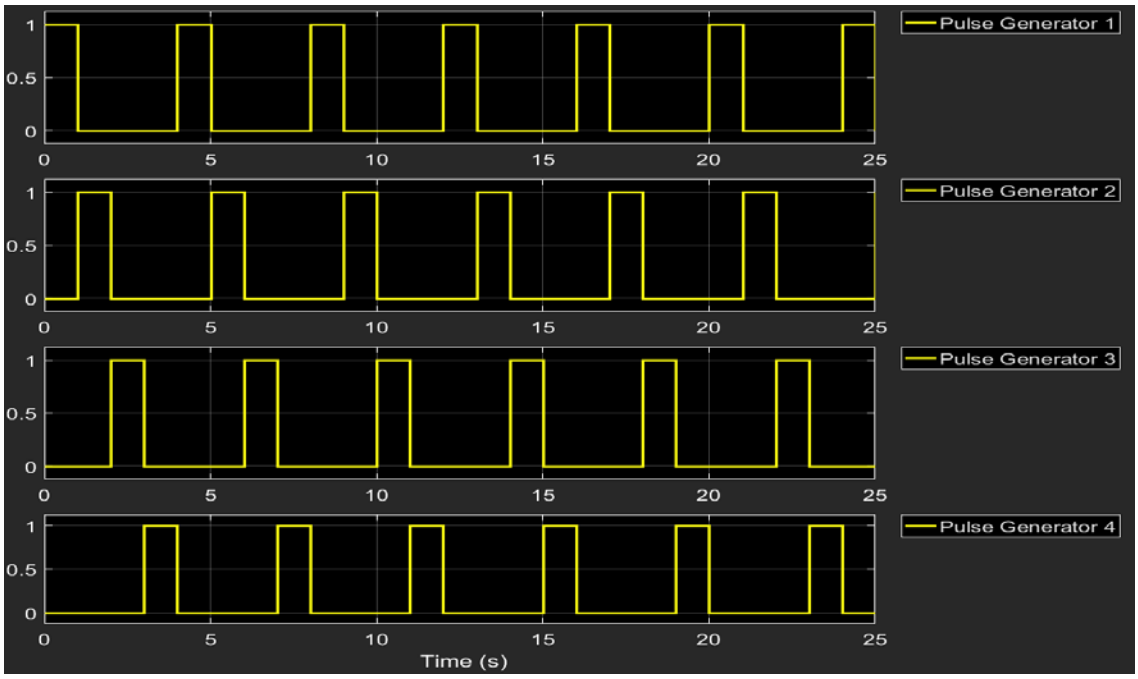

Figure 14. Generated 4-PPM Pulses

The 4-PPM signal appears at the output of the multiport switch. The signal is shown in Figure 15. Depending on the integer numbers provided by the random integer generator, these pulses change every time the simulation is run. Note that there is only one pulse in each symbol period.

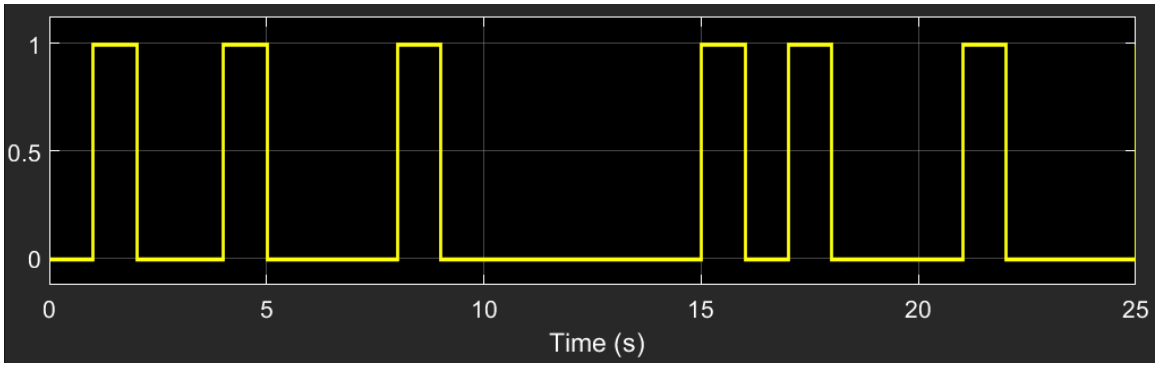

Figure 15. 4-PPM Signal

The *M*-ary PPM modulator block for 8-PPM is shown in Figure 16. The 8-PPM modulator block consists of eight pulse generators instead of four. Pulse generator 1 is

connected to the multiport switch without delay. Pulse generators 2, 3, 4…8 delay the signal T, $2T$, $3T$…$7T$ seconds, respectively. A random integer generator provides eight random integers to the multiport switch through port In1.

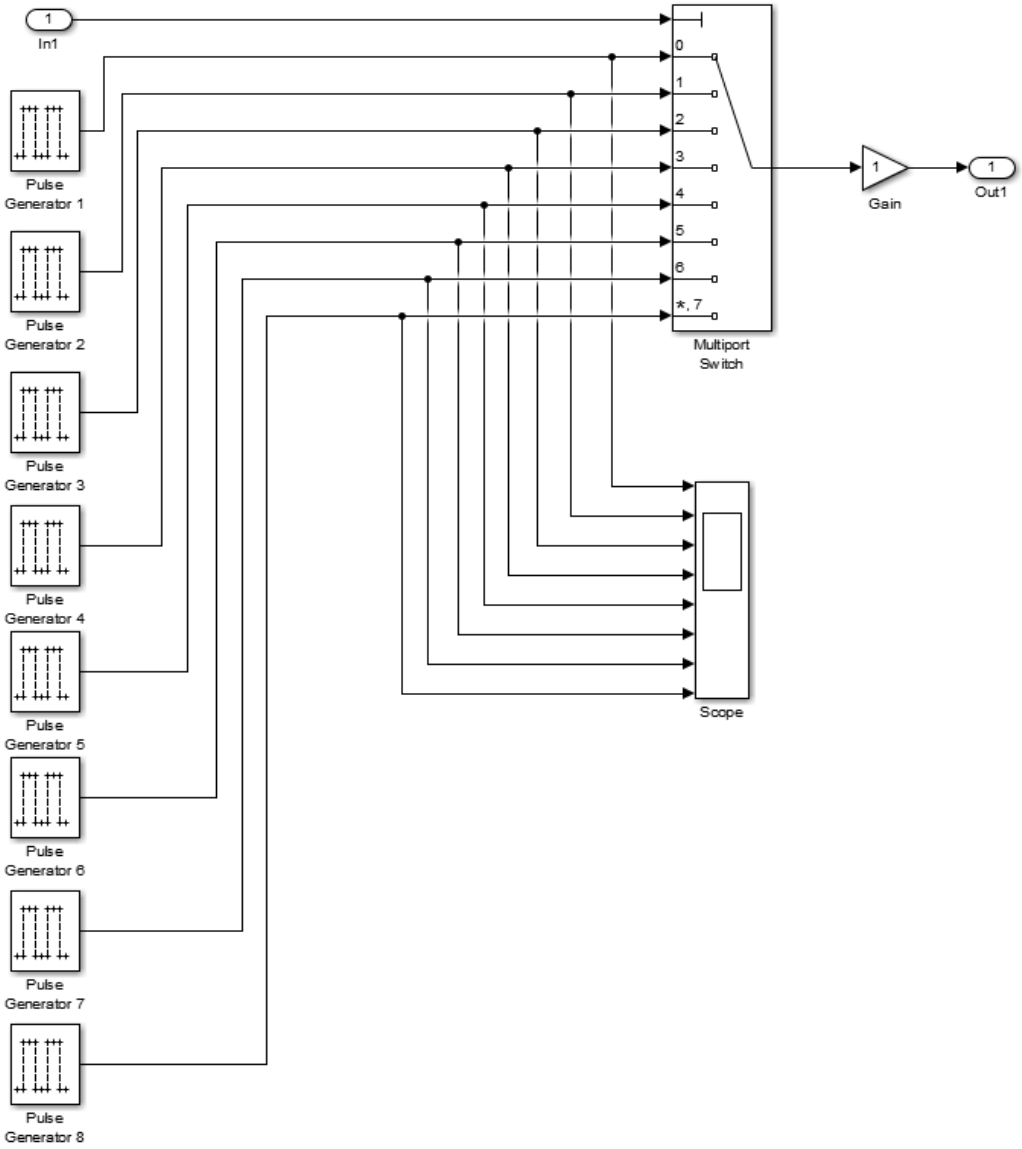

Figure 16. 8-PPM Modulator Block

An example of generated 8-PPM pulses is shown in Figure 17. The pulse generators generate the same pulse every $8T$ seconds.

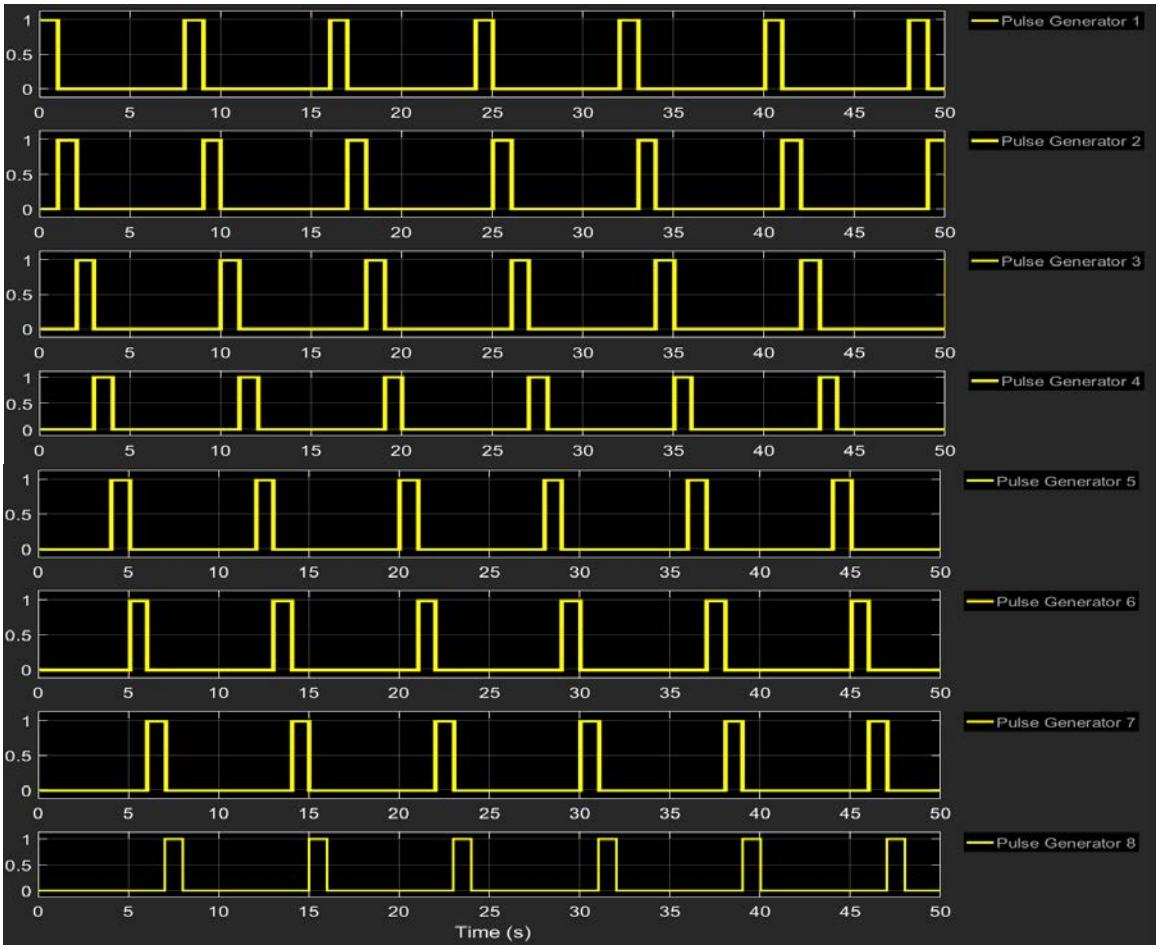

Figure 17. Generated 8-PPM Pulses

The 8-PPM signal is shown in Figure 18. Note that there is only one pulse in every symbol period of 8*T* seconds. The simulation is run for a 50-second period for 8-PPM.

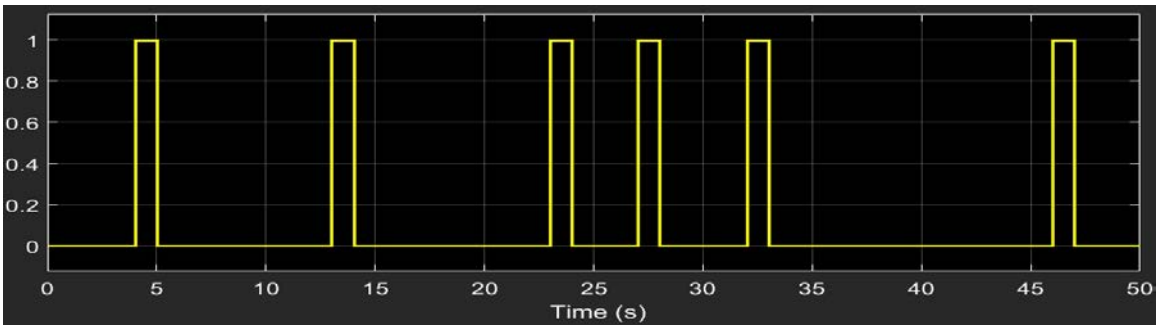

Figure 18. 8-PPM Signal

The 16-PPM modulator block is shown in Figure 19 and consists of 16 pulse generators. A random integer generator provides 16 random integers to the multiport switch through port In1. Delay values for the pulse generators are adjusted in the same way as for the 8-PPM modulator pulse generators.

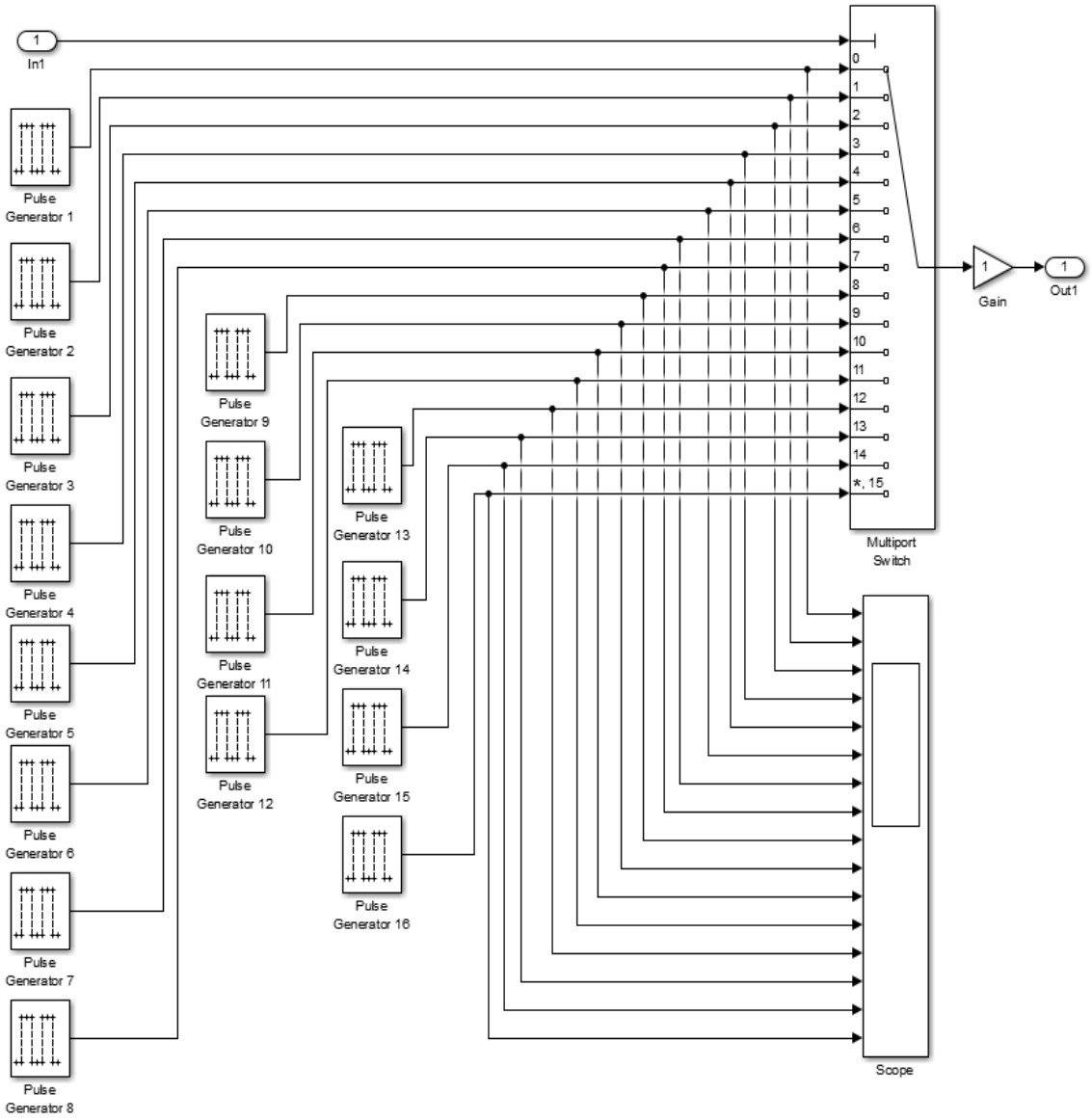

Figure 19. 16-PPM Modulator Block

B. SIMULATION OF *M*-ARY PPM DIRECT DETECTION IN SIMULINK

The *M*-ary PPM modulation and demodulation general design is shown in Figure 20. The *M*-ary PPM signal is fed to a *M*-ary PPM demodulator after it is generated. Note that the channel is not included in the simulation; hence, the channel is assumed to be free space. We intend to confirm the power efficiency of *M*-ary PPM over OOK modulation. The laser transmitter and optical receiver are assumed to be perfect.

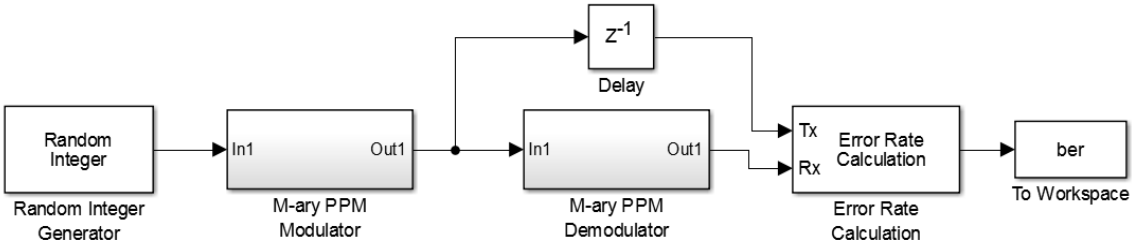

Figure 20. *M*-ary PPM Simulation General Design

The error ratio calculator compares transmitted and received signals to calculate the BER. The transmitted signals are delayed one *T* time slot to synchronize the transmitted signal with the received signal. The output of the error ratio calculator is sent to the Matlab workspace to plot the BER.

The *M*-ary PPM demodulator block is shown in Figure 21. This block is the same for all *M* for *M*-ary PPM demodulation. This means that the design does not need to be changed for different *M*.

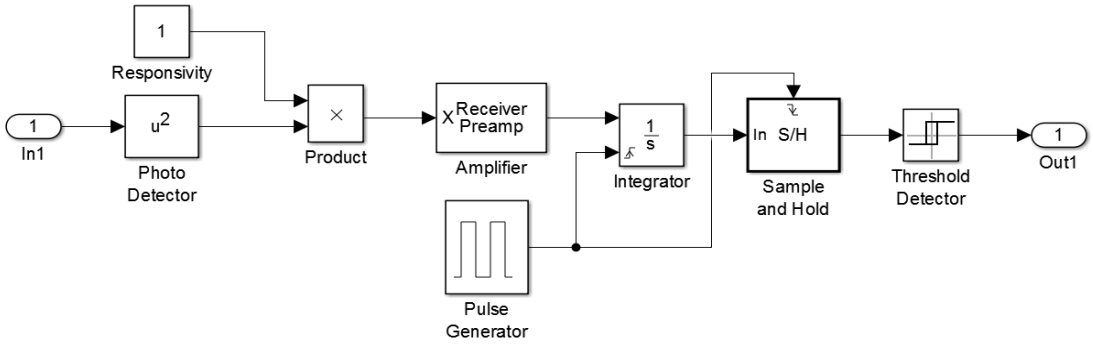

Figure 21. *M*-ary PPM Demodulator Block

In this simulation, we used “square,” a math function, to simulate the photo detector. The responsivity of the photo detector was assumed to be 1.0 A/W.

The received *M*-ary PPM signal is squared and fed to the amplifier. The amplification is set to 0 dB. Amplifier noise power is set to different values to calculate BER, which is explained later.

After amplification, the received signal is integrated by a continuous-time integrator. To integrate the signal every *T* seconds, a continuous-time pulse generator signal is used to trigger the integrator. The pulse generator triggers the integrator by sending pulses with a *T*-second duration. As a result, the integrator resets itself every *T* seconds; otherwise, the integrator continues integrating the signal, which is not desired.

The sample-and-hold block samples the signal every *T* seconds. It takes the highest value of the received signal and holds its output at that level for *T* seconds. The sample-and-hold block is also triggered by the same pulse generator to keep sampling the signal for every *T* seconds.

Lastly, the threshold detector lets through the pulses that are greater than the threshold voltage. The threshold voltage is set to 0.5 V. The detector outputs 0 and 1 as appropriate.

The demodulation process is presented step-by-step in Figure 22 for an 8-PPM signal. The noise power of the amplifier is set to zero. Note that the recovered signal is delayed by one *T* second. This is the desired outcome. This delay is caused by the sample-and-hold block since the sample-and-hold block starts sampling after the integrated signal reaches its largest value.

The demodulation process with thermal noise is shown in Figure 23. The thermal noise power is set to -15 dBW. It can be seen that the noise distorts the signal, but the signal is recovered without error with the help of integration, sampling, and threshold detection. Note that the noise is added to the signal before integration.

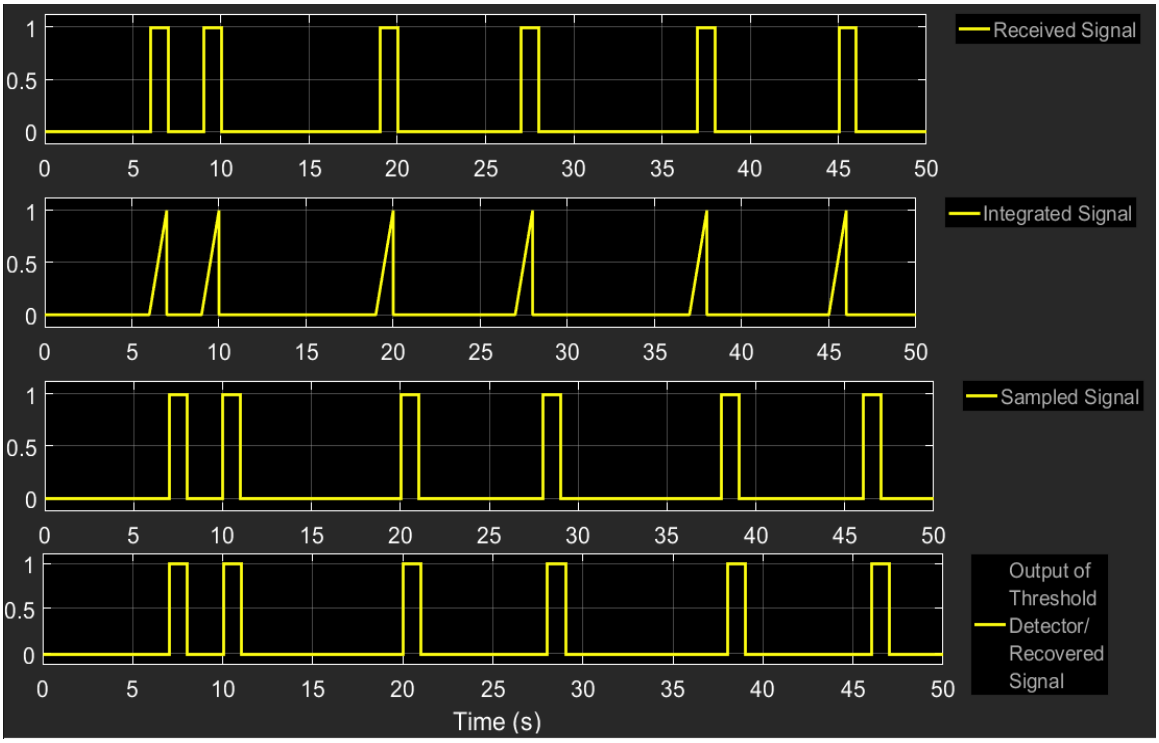

Figure 22. Demodulation Process of 8-PPM

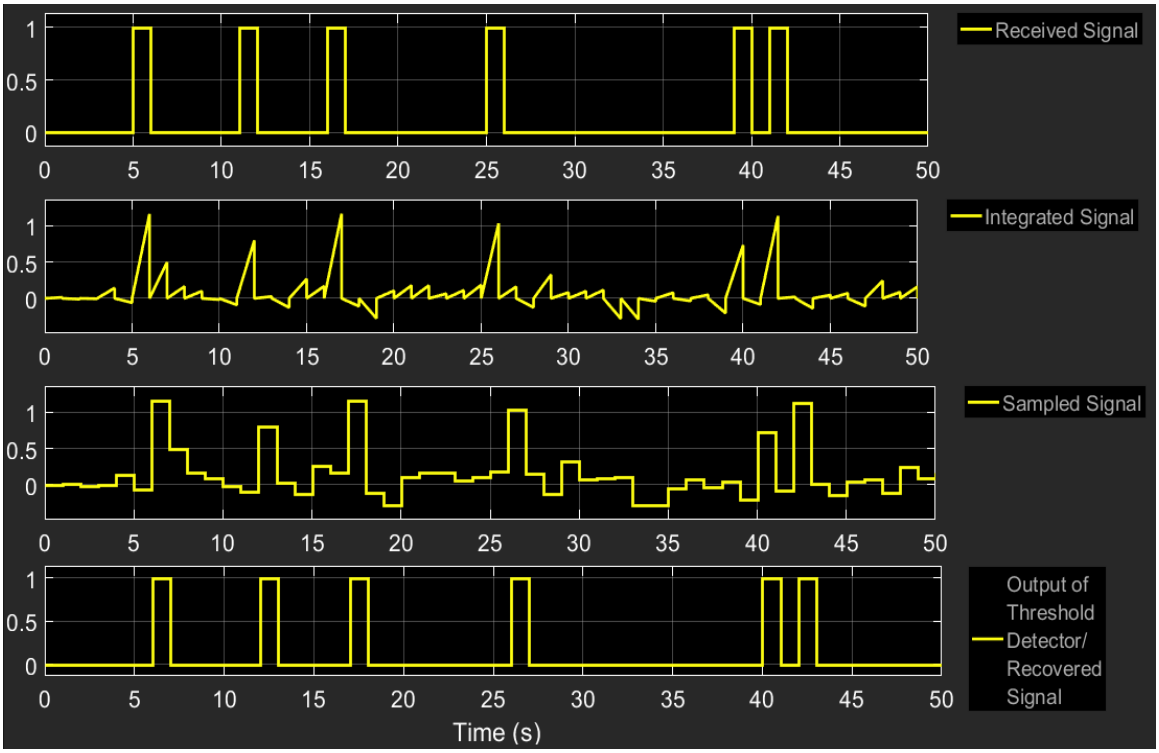

Figure 23. Demodulation Process of 8-PPM with Thermal Noise

Adjusting the threshold voltage is important in order to decrease the number of errors in the demodulation process. The demodulation process is presented in Figure 24 when the threshold voltage is lowered from 0.5 V to 0.3 V. It can be seen that there are three errors in the recovered signal. Note that thermal noise remains at the same at -15 dBW.

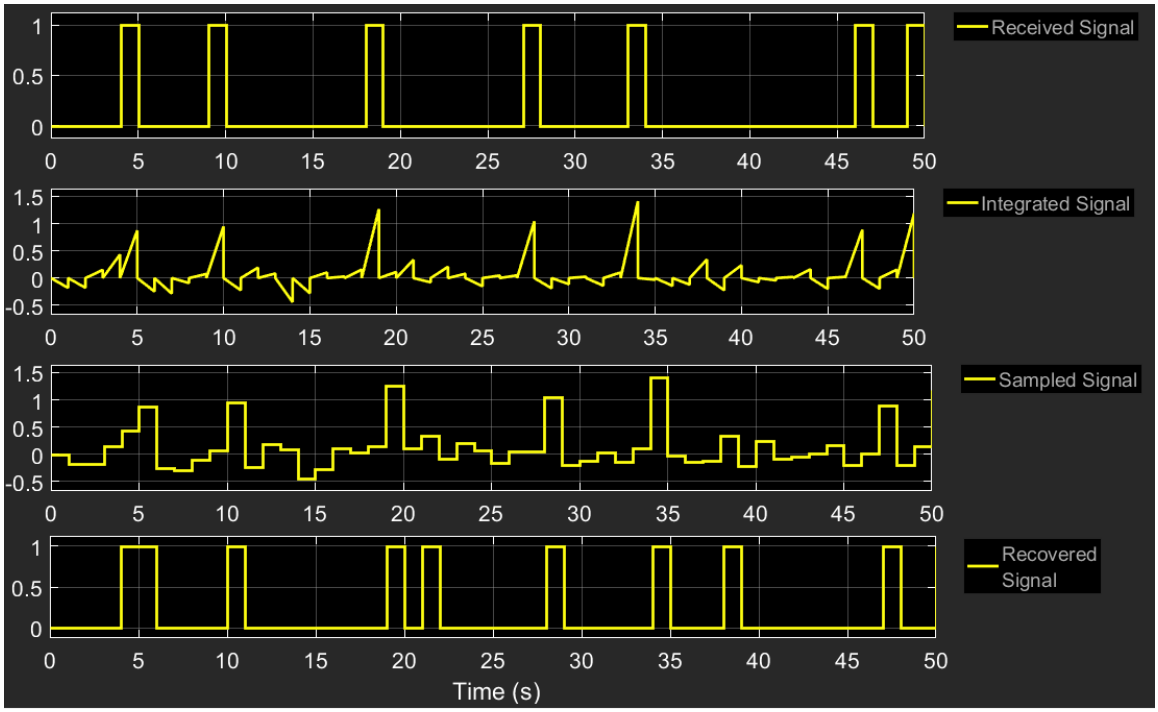

Figure 24. Demodulation Process with Different Threshold Voltage

C. PERFORMANCE ANALYSIS OF *M*-ARY PPM IN SIMULINK

The thermal noise generated by the amplifier causes the demodulation process to produce errors. To the find the average power requirement for *M*-ary PPM, the 4-PPM simulator was run for different thermal noise power values ranging from -20 dBW to 0 dBW. The simulation results for different noise powers and BERs are shown in Table 5. Note that the amplification is set to 0 dB. It can be seen that as the noise power decreases, the BER decreases.

The received *M*-ary PPM signal was integrated to calculate the average power requirement. The 4-PPM had a total power of 25 W when the simulation was run for 100

seconds. The 8-PPM had a total power of 12.5 W. The 16-PPM had a total power of 6.25 W.

Table 5. 4-PPM BER Calculation Results

Noise Power (dBW)	BER	Noise Power (dBW)	BER
0	2.83×10^{-1}	-11	3.86×10^{-2}
-1	2.88×10^{-1}	-12	2.29×10^{-2}
-2	2.65×10^{-1}	-13	1.3×10^{-2}
-3	2.4×10^{-1}	-14	5.7×10^{-3}
-4	2.21×10^{-1}	-15	2.3×10^{-3}
-5	1.91×10^{-1}	-16	7.2×10^{-4}
-6	1.58×10^{-1}	-17	1.8×10^{-4}
-7	1.32×10^{-1}	-18	3×10^{-5}
-8	1.04×10^{-1}	-19	3×10^{-6}
-9	7.91×10^{-2}	-20	2.1×10^{-7}
-10	5.59×10^{-2}		

The average total power conforms to the average power for the *M*-ary PPM signal, $A^2/2M$. Using 4-PPM noise power and BER, we computed SNR. The average received power is assumed to be constant during SNR calculation.

The average received power requirement calculation using the post-photo detector SNR for FSO systems is given by [17]

$$P = \frac{1}{\Re}\sqrt{\sigma_N^2 SNR}, \tag{4-1}$$

where σ_N^2 is the noise power and $\Re$ is the photo-detector responsivity. Note that the average received power is defined at the photo-detector input. On the other hand, the signal power in SNR is defined at the integrator input. These two qualities are different. In fact, the average received power equals the ratio of the square root of the signal power in SNR to the photo-detector responsivity. This can be seen from (4-1). Note that the photo detector is modeled as a square-law device, and amplifier noise is added after the photo detection. This is the difference between optical direct detection and RF noncoherent detection where noise is added before the square-law device.

The average received power requirement for 4-PPM are calculated using (4-1). The average received power requirements for 2-PPM, 8-PPM, 16-PPM, and 32-PPM were then scaled using (3-38). The average received power requirement for OOK modulation was scaled using (3-41).

The average power requirements presented in Figure 11 were calculated for simulation values. The noise spectrum was normalized in order to present theoretical and simulation results on the same plot. The responsivity value of 0.7 A/W is included in both theoretical and simulation result calculations. Extinction ratio r_e was set to zero for the theoretical calculations. Results are shown in Figure 25.

It can be seen from Figure 25 that 4-PPM has a 1.4 dB power gain over OOK, while 8-PPM, 16-PPM, and 32-PPM have 3.7 dB, 5.7 dB and 7.6 dB power gain over OOK, respectively, at $P_b = 10^{-6}$.

The *M*-ary PPM BER versus SNR plot for both theoretical and simulation results is shown in Figure 26. To convert average power values to SNR for theoretical results, (4-1) was used. The Matlab codes for Figure 25 and Figure 26 are presented in the appendix.

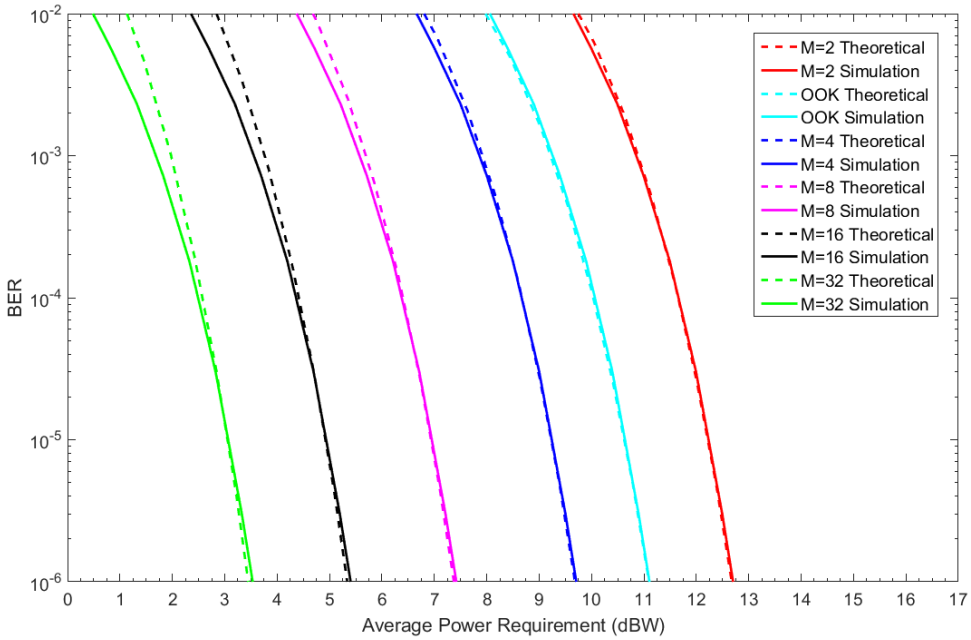

Figure 25. *M*-ary PPM and OOK Power Requirement Comparison of Simulation and Theoretical Results

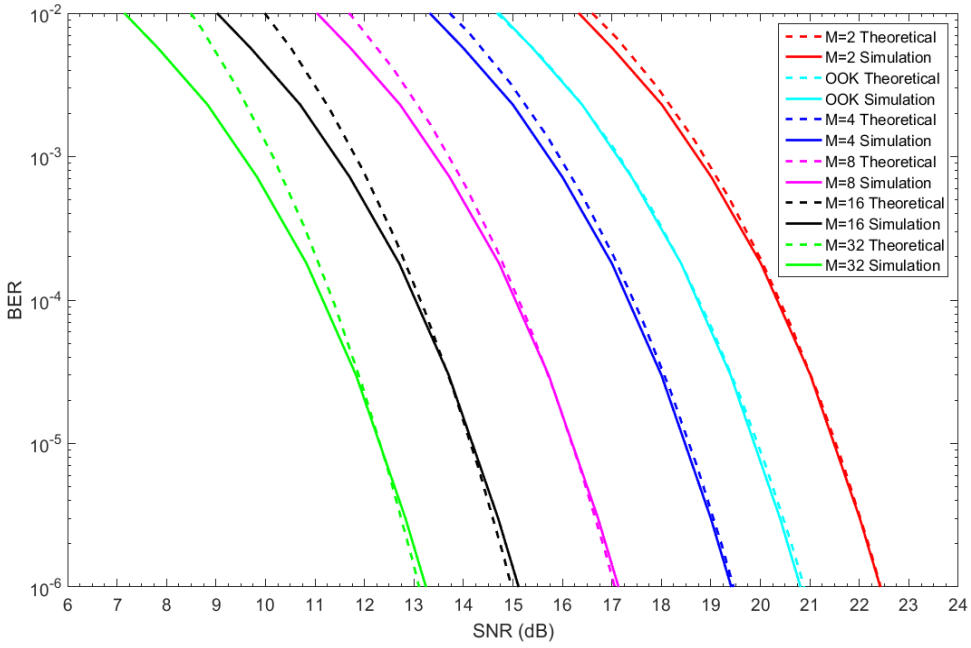

Figure 26. *M*-ary PPM and OOK SNR Comparison of Simulation and Theoretical Results

D. CONCLUSION

In this chapter, *M*-ary PPM modulation and demodulation with direct detection method were simulated in Simulink. Simulation blocks and their roles were explained. The effects of the thermal noise and threshold voltage on the demodulation process were presented. The BERs for different noise powers were calculated. Total received power for different *M*-ary PPM were obtained, and a performance comparison of *M*-ary PPM and OOK was presented.

The simulation results confirm that the analytical results in Chapter III are valid; *M*-ary PPM is much more power efficient than OOK modulation.

V. CONCLUSIONS

A. SUMMARY OF RESULTS

Low power and inexpensive lasers were analyzed in this thesis. The effect of background radiation was examined, and an optical communications link analysis for different wavelengths of the optical signal was presented. Optical link distance and bit rate for low-power lasers were researched. It was found that an optical signal with a 600 nm wavelength provides a better link distance than an optical signal with a 1550 nm wavelength. Although using an optical signal with a 600 nm wavelength is limited by eye and skin safety regulations, it is not an issue for low power, inexpensive lasers. Additionally, possible ways to improve link distance and bit rate were explained.

M-ary PPM with direct detection demodulation was investigated. *M*-ary PPM was compared with OOK in terms of power efficiencies. It was found that *M*-ary PPM uses significantly less power than OOK. Considering the fact that a laser transmitter with 1.0 W output power is ten times more expensive than a laser transmitter with 250 mW output power, the power efficiency of *M*-ary PPM makes it a very attractive choice when using low power, inexpensive lasers.

A simulation for *M*-ary PPM with direct detection demodulation was designed in Simulink for different *M* to confirm theoretical results with a simulation. The simulation was run for different thermal noise levels to obtain the BER. Average power requirements and SNR plots for both theoretical and simulation results were presented. It was found that the simulation results confirm the power efficiency of *M*-ary PPM.

B. RECOMMENDATIONS FOR FUTURE WORK

It is possible to increase optical communication link distance and bit rate using error correction coding. The coding gain is estimated to be 4 to 6 dB. It is also possible to use lasers that have smaller beam divergence angles to increase link distance and bit rate. Laser transmitters with different beam divergence angles can be analyzed to see how they change the link distance and bit rate.

In our analysis, we used a photo detector with a PIN diode, which has low gain, to detect optical signal; photo detectors with an APD diode have a higher gain and a higher cost. Link analysis for photo detectors with APD diodes show the possible link distance increases, but there are trade-offs given their high cost.

Optical communication link analysis in this thesis was made assuming that the optical link is in an atmospheric channel. An optical link analysis in underwater conditions could reveal possibilities for underwater applications.

Tracking an optical signal is one of the biggest challenges for optical communications. Most of the platforms considered for optical communications are either stationary or have consistent movement; however, an application for ship-to-ship optical communication could be a very good alternative for high-speed communications.

APPENDIX. MATLAB CODES

A. AVERAGE POWER CALCULATION

Matlab code for the calculation of the average power requirements for both the simulation and theoretical results shown in Figure 25 is given in this appendix.

```
n=3.6; % normalized noise spectrum
re=0; % extinction ratio
r=0.7; % responsivity of photo detector
ppo=0:1:100; % ook average power
load ber.mat; % 4-PPM ber values from simulation
load snr.mat; % 4-PPM snr values from simulation
pow_norm=sqrt(10.^(snr./10))./1;%snr to average power conversion
pow_norm_ook=pow_norm.*1.38; %OOK power

% 2-PPM Theoretical Calculation
tb=0.5; %bit time
m=2;
ppm=(ppo.*1.444); % 2-PPM average power
ppmdb=10*log10(ppm); % dB conversion
prp=qfunc(((r.*(10.^(ppmdb./10)).*m*(1-
re))./(2*(1+re))).*(sqrt(tb/n)))*((m*(m+1))/(4*(m-1))); % probability of bit error
semilogy(ppmdb,prp,'r--','LineWidth',2)
hold on

% 2-PPM Simulation Calculation
pow_db=10*log10(pow_norm_ook.*1.444);
semilogy(pow_db,ber,'r','LineWidth',2)

%OOK Theoretical
tb=1;
ppodb=10*log10(ppo);
pro=qfunc(((r.*(10.^(ppodb./10)).*(1-re))./(1+re)).*(sqrt((tb)/(n))));
semilogy(ppodb,pro,'c--','LineWidth',2)

% OOK Simulation
pow_db=10*log10(pow_norm_ook);
semilogy(pow_db,ber,'c','LineWidth',2)

% 4-PPM Theoretical
tb=0.5;
```

```
m=4;
ppm=ppo.*0.725;
ppmdb=10*log10(ppm);
prp=qfunc(((r.*(10.^(ppmdb./10)).*m*(1-
re))./(2*(1+re))).*(sqrt(tb/n)))*((m*(m+1))/(4*(m-1)));
semilogy(ppmdb,prp,'b--','LineWidth',2)

% 4-PPM Simulation
pow_db=10*log10(pow_norm_ook.*0.725);
semilogy(pow_db,ber,'b','LineWidth',2)

% 8-PPM Theoretical
tb=3/8;
m=8;
ppm=ppo.*0.428;
ppmdb=10*log10(ppm);
prp=qfunc(((r.*(10.^(ppmdb./10)).*m*(1-
re))./(2*(1+re))).*(sqrt(tb/n)))*((m*(m+1))/(4*(m-1)));
semilogy(ppmdb,prp,'m--','LineWidth',2)

% 8-PPM Simulation
pow_db=10*log10(pow_norm_ook.*0.428);
semilogy(pow_db,ber,'m','LineWidth',2)

% 16-PPM Theoretical
tb=0.25;
m=16;
ppm=ppo.*0.269;
ppmdb=10*log10(ppm);
prp=qfunc(((r.*(10.^(ppmdb./10)).*m*(1-
re))./(2*(1+re))).*(sqrt(tb/n)))*((m*(m+1))/(4*(m-1)));
semilogy(ppmdb,prp,'k--','LineWidth',2)

% 16-PPM Simulation
pow_db=10*log10(pow_norm_ook.*0.269);
semilogy(pow_db,ber,'k','LineWidth',2)

% 32-PPM Theoretical
tb=5/32;
m=32;
ppm=ppo.*0.1749;
ppmdb=10*log10(ppm);
prp=qfunc(((r.*(10.^(ppmdb./10)).*m*(1-
re))./(2*(1+re))).*(sqrt(tb/n)))*((m*(m+1))/(4*(m-1)));
semilogy(ppmdb,prp,'g--','LineWidth',2)
```

```
 % 32-PPM Simulation
pow_db=10*log10(pow_norm_ook.*0.1749);
semilogy(pow_db,ber,'g','LineWidth',2)

xlabel('Average Power Requirement (dBW)')
ylabel('BER')
ylim([10e-7 10e-3])
xlim([0 17])
legend('M=2 Theoretical','M=2 Simulation','OOK Theoretical','OOK Simulation','M=4
Theoretical','M=4 Simulation','M=8 Theoretical','M=8 Simulation','M=16
Theoretical','M=16 Simulation','M=32 Theoretical','M=32 Simulation')
```

B. SNR CALCULATION

Matlab code for calculation of the SNR for simulation and theoretical results shown in Figure 26 is presented below.

```
n=7.5; % normalized noise spectrum
re=0; % extinction ratio
r=0.7; % responsivity of photo detector
ppo=0:1:100; % ook average power
load ber.mat; % 4-PPM ber values from simulation
load snr.mat; % 4-PPM snr values from simulation
snr_norm=10.^(snr./10); %normal snr values

% 2-PPM Theoretical Calculation
tb=0.5; %bit time
m=2;
ppm=(ppo.*1.444); % 2-PPM average power
ppmdb=10*log10(ppm); % dB conversion
prp=qfunc(((r.*(10.^(ppmdb./10)).*m*(1-
re))./(2*(1+re))).*(sqrt(tb/n)))*((m*(m+1))/(4*(m-1))); % probability of bit error
ppmdb=10*log10(((ppm.*r).^2)/2); % power to snr conversion
semilogy(ppmdb,prp,'r--','LineWidth',2)
hold on

% 2-PPM Simulation Calculation
snr_db=10*log10(snr_norm./0.5);
semilogy(snr_db,ber,'r','LineWidth',2)

%OOK Theoretical
tb=1;
ppodb=10*log10(ppo);
```

```
pro=qfunc(((r.*(10.^(ppodb./10)).*(1-re))./(1+re)).*(sqrt((tb)/(n))));
ppodb=10*log10(((ppo.*r).^2)/1.38);
semilogy(ppodb,pro,'c--','LineWidth',2)

% OOK Simulation
snr_db=10*log10(snr_norm.*1.38);
semilogy(snr_db,ber,'c','LineWidth',2)

% 4-PPM Theoretical
tb=0.5;
m=4;
ppm=ppo.*0.725;
ppmdb=10*log10(ppm);
prp=qfunc(((r.*(10.^(ppmdb./10)).*m*(1-
re))./(2*(1+re))).*(sqrt(tb/n)))*((m*(m+1))/(4*(m-1)));
ppmdb=10*log10(((ppm.*r).^2)/1);
semilogy(ppmdb,prp,'b--','LineWidth',2)

% 4-PPM Simulation
snr_db=10*log10(snr_norm);
semilogy(snr_db,ber,'b','LineWidth',2)

% 8-PPM Theoretical
tb=3/8;
m=8;
ppm=ppo.*0.428;
ppmdb=10*log10(ppm);
prp=qfunc(((r.*(10.^(ppmdb./10)).*m*(1-
re))./(2*(1+re))).*(sqrt(tb/n)))*((m*(m+1))/(4*(m-1)));
ppmdb=10*log10(((ppm.*r).^2)/0.6);
semilogy(ppmdb,prp,'m--','LineWidth',2)

% 8-PPM Simulation
snr_db=10*log10(snr_norm./1.69);
semilogy(snr_db,ber,'m','LineWidth',2)

% 16-PPM Theoretical
tb=0.25;
m=16;
ppm=ppo.*0.269;
ppmdb=10*log10(ppm);
prp=qfunc(((r.*(10.^(ppmdb./10)).*m*(1-
re))./(2*(1+re))).*(sqrt(tb/n)))*((m*(m+1))/(4*(m-1)));
ppmdb=10*log10(((ppm.*r).^2)/0.38);
semilogy(ppmdb,prp,'k--','LineWidth',2)
```

```
% 16-PPM Simulation
snr_db=10*log10(snr_norm./2.69);
semilogy(snr_db,ber,'k','LineWidth',2)

% 32-PPM Theoretical
tb=5/32;
m=32;
ppm=ppo.*0.1749;
ppmdb=10*log10(ppm);
prp=qfunc(((r.*(10.^(ppmdb./10)).*m*(1-
re))./(2*(1+re))).*(sqrt(tb/n)))*((m*(m+1))/(4*(m-1)));
ppmdb=10*log10(((ppm.*r).^2)/0.245);
semilogy(ppmdb,prp,'g--','LineWidth',2)

% 32-PPM Simulation
snr_db=10*log10(snr_norm./4.14);
semilogy(snr_db,ber,'g','LineWidth',2)

xlabel('SNR (dB)')
ylabel('BER')
ylim([10e-7 10e-3])
xlim([7 26])
legend('M=2 Theoretical','M=2 Simulation','OOK Theoretical','OOK Simulation','M=4
Theoretical','M=4 Simulation','M=8 Theoretical','M=8 Simulation','M=16
Theoretical','M=16 Simulation','M=32 Theoretical','M=32 Simulation')
```

THIS PAGE INTENTIONALLY LEFT BLANK

LIST OF REFERENCES

[1] A. K. Majumdar and J. C. Ricklin, *Free-Space Laser Communications: Principles and Advances*. New York, NY: Springer, 2008.

[2] F. Fidler, "Optical communications from high-altitude platforms," Ph.D. dissertation, Dept. Elect. Eng., Vienna Univ. Tech., Vienna, Austria, 2007.

[3] J. Kahn and J. Barry, "Wireless infrared communications," *Proc. IEEE*, vol. 85, no. 2, pp. 265–298, Feb. 1997.

[4] H. Hemmati, *Near-Earth Laser Communications*. Boca Raton: CRC Press, 2009.

[5] A. K. Majumdar, *Advanced Free Space Optics (FSO): A Systems Approach*. New York, NY: Springer, 2015.

[6] K. Rainey. (2014, Dec. 9). OPALS: Light beams let data rates soar [Online]. Available: http://www.nasa.gov/mission_pages/station/research/news/opals_data_rates_soar

[7] B. J. Klein and J. J. Degnan, "Optical antenna gain 1: Transmitting antennas," *Appl. Opt.*, vol. 13, no. 9, pp. 2134–2141, Sept. 1974.

[8] A. E. Siegman, *An Introduction to Lasers and Masers*. New York: McGraw-Hill Book Company, 1972.

[9] T. T. Ha, W. Su and R. Romero, "Free-space optical communications," Naval Postgraduate School, Monterey, CA, Tech. Rep., Oct. 2015.

[10] W. K. Pratt, *Laser Communication Systems*. New York: Wiley, 1969.

[11] W. R. Leeb, "Degradation of signal to noise ratio in optical free space data links due to background illumination," *Appl. Opt.*, vol. 28, no. 15, pp. 3443–3449, Aug. 1989.

[12] M. Pfennigbauer, "Design of optical space-to-ground links for the international space station," Ph.D. dissertation, Dept. Elect. Eng., Vienna Univ. Tech., Vienna, Austria, 2004.

[13] A. E. Roy and D. Clarke, *Astronomy, Principles and Practice*, 4th ed. Philadelphia: Inst. of Phys. Pub., 2003.

[14] T. T. Ha, *Theory and Design of Digital Communication Systems*. New York: Cambridge University Press, 2011.

[15] M. Audeh and J. Kahn, “Performance evaluation of L-pulse-position modulation on non-directed indoor infrared channels,” in *Proceedings of International Conference on Communications*, New Orleans, 1994, vol. 2, pp. 660–664.

[16] Z. Ghassemlooy, W. Popoola, and S. Rajbhandari, *Optical Wireless Communications: System and Channel Modelling with MATLAB*. Boca Raton, FL: Taylor & Francis, 2012.

[17] T. Y. Elganimi, “Performance comparison between OOK, PPM, and PAM modulation schemes for free space optical (FSO) communication systems: Analytical study,” *Int. J. of Comput. Appl.*, vol. 79, no. 11, pp. 22–27, Oct. 2013.

INITIAL DISTRIBUTION LIST

1. Defense Technical Information Center
   Ft. Belvoir, Virginia

2. Dudley Knox Library
   Naval Postgraduate School
   Monterey, California